A novel coordinated function of Myosin II with GOLPH3 controls centralspindlin localization during cytokinesis

Stefano Sechi[1,¶], Anna Frappaolo[1,¶], Angela Karimpour-Ghahnavieh[1], Roberta Fraschini[2] and Maria Grazia Giansanti[1,*]

[1]Istituto di Biologia e Patologia Molecolari del CNR, Dipartimento di Biologia e Biotecnologie, Università Sapienza di Roma, Piazzale A. Moro 5, 00185 Roma, Italy.

[2]Dipartimento di Biotecnologie Bioscienze, Università degli Studi di Milano Bicocca, 20126, Milano, Italy.

[¶] These authors contributed equally to this work.
[*]Corresponding author: Maria Grazia Giansanti
E mail: mariagrazia.giansanti@uniroma1.it (MGG)

Keywords: Drosophila, male meiosis, cytokinesis, Myosin, GOLPH3

Summary statement

We show that during cytokinesis non-muscle Myosin II controls centralspindlin maintenance at the cleavage furrow and actomyosin ring constriction by recruiting the Phosphatidylinositol 4-phosphate binding protein GOLPH3.

Abstract

In animal cell cytokinesis interaction of non-muscle Myosin II (NMII) with F-actin provides the dominant force for pinching the mother cell into two daughters. Here we demonstrate that *celibe (cbe)* is a missense allele of *zipper*, which encodes the *Drosophila* Myosin heavy chain. *cbe* mutation impairs binding of Zipper protein to the regulatory light chain Spaghetti Squash (Sqh). In dividing spermatocytes from *cbe* males, Sqh fails to concentrate at the equatorial cortex, resulting in thin actomyosin rings that are unable to constrict. We show that *cbe* mutation impairs localization of the Phosphatidylinositol 4-phosphate [PI(4)P] binding protein Golgi phosphoprotein 3 (GOLPH3) and maintenance of centralspindlin at the cell equator of telophase cells. Our results further demonstrate that GOLPH3 protein associates with Sqh and directly binds the centralspindlin subunit Pavarotti. We propose that during cytokinesis the reciprocal dependence between Myosin and PI(4)P-GOLPH3 regulates centralspindlin stabilization at the invaginating plasma membrane and contractile ring assembly.

Introduction

Animal cell cytokinesis is accomplished by constriction of the contractile ring at the equatorial cortex (D'Avino et al., 2015). After anaphase onset, a structure composed by non-muscle Myosin II (NMII) and filamentous actin (F-actin) is assembled just beneath the plasma membrane, providing the dominant force for pinching the dividing cell into two daughter cells. Three different genes in mammalian cells encode the NMII heavy chain (NMHC II) proteins whereas only one gene encodes the *Drosophila* NMHC II protein Zipper (Zip) (Ketchum et al., 1990; Kiehart et al., 1989; Mansfield et al., 1996; Young et al., 1993).

The NMII molecule is a hexamer composed of two identical heavy chains, a pair of essential light chains (ELC) and a pair of regulatory light chains (RLC; Shutova and Svitkina, 2018, Fig. 1A). Each heavy chain contains a conserved N-terminal globular head domain with the ATPase and the actin binding activity. One RLC and one ELC associate with each NMHC II via two IQ motifs on a neck region that connects the head and tail domains (Fig. 1A). The NMHC II C-terminus has a long coiled-coil tail domain responsible for the assembly of NMII monomers into bipolar filaments (Murakami et al.; 2000; Ronen and Ravid, 2009; Shutova and Svitkina, 2018; Vincente-Manzanares et al., 2009). Studies in multiple model systems demonstrated the essential role for NMHC II for normal cytokinesis (De Lozanne and Spudich, 1987; Echard et al., 2004; Eggert et al., 2004; Hickson

et al., 2006; Ma et al., 2012; Mabuchi and Okuno, 1977; Osorio et al., 2019; Straight et al., 2003; Straight et al., 2005; Wang et al., 2019). Analysis of myosin truncations revealed that targeting NMHC II to the cleavage furrow does not require the motor domain but involves signals in the tail (Beach and Egelhoff, 2009; Uehara et al., 2010). Total reflection fluorescence imaging of the cortex of *Drosophila* S2 dividing cells showed that NMII filaments are highly dynamic, suddenly concentrating at the equatorial cortex and disappearing from the poles (Vale et al., 2009). According to the most widely accepted model for NMII recruitment, *de novo* filament assembly occurs at the equatorial cortex via localized RLC phosphorylation, stimulated by the Rho pathway. During late anaphase, the small GTPase RhoA/Rho1 stimulates F-actin filament formation in the cortex and controls contractile ring constriction by activating Rho kinase which phosphorylates RLC on Thr-18/Ser-19 (Eda et al., 2001; Ishizaki et al., 1996; Matsumura et al., 2011; Yamashiro et al., 2003). The evolutionarily conserved two-protein complex centralspindlin, composed of two molecules of the kinesin family member MKLP1/Pavarotti (Pav) and two molecules of the Rho family GAP CYK-4/RacGAP50C, has key role in specifying the site of the cleavage furrow (D'Avino et al., 2006, 2015; Giansanti and Fuller; 2012). The balance between the active state (GTP-bound) and inactive state (GDP-bound) of RhoA/Rho1 requires the recruitment of the RhoGEF ECT2/Pebble to the equatorial cortex, which is mediated by centralspindlin (Kamijo et al., 2006; Nishimura and Yonemura, 2006; Piekny et al., 2005; Somers and Saint, 2003; Yuce et al., 2005; Zhao and Fang, 2005).

Recent work suggests that the interaction with plasma membrane lipids might have an important role in localizing centralspindlin as well as NMII at the cleavage furrow (Basant et al., 2015; Lekomtsev et al., 2012; Liu et al., 2016). The centralspindlin subunit HsCyk-4/MgcRacGAP binds to PI(4)P and PI(4,5)P2 phosphoinositides at the furrow plasma membrane via its C1 domain (Lekomtsev et al., 2012). Mammalian NMIIA, NMIIB and NMIIC bind to negatively charged liposomes containing one or more acidic phospholipids and NMIIA associates with plasma membrane of HeLa cells and fibrosarcoma when actin filaments are depolymerized (Liu et al., 2016). Moreover RLC interacts with Phosphatidylinositol 4-Phosphate [PI(4)P] and mediates plasma membrane localization of PI(4)P in dividing neuroblasts (Koe et al., 2018). In this context, we previously demonstrated that the PI(4)P binding protein GOLPH3 is required to stabilize NMII rings and to maintain centralspindlin at the cell equator of dividing cells in *Drosophila melanogaster* (Sechi et al., 2014).

Here we show that *celibe (cbe),* identified during a screen for mutants affecting spermatocyte cytokinesis (Giansanti et al., 2004), is a missense allele of *Drosophila zipper* affecting contractile ring structure in both mitotic and meiotic cells. In *cbe* mutants, Zip protein is unable to bind the RLC protein Spaghetti Squash (Sqh). *cbe* mutant spermatocytes display initial localization of Zip and

Septin proteins at the cleavage site during late anaphase-early telophase but do not concentrate Sqh at the equatorial cortex. However, the contractile rings assembled in *cbe* mutant spermatocytes appear thin, fail to constrict and fragment during later stages of cytokinesis. We further show that *cbe* mutation impairs localization of GOLPH3 and maintenance of centralspindlin at the clevage furrow. We demonstrate that GOLPH3 protein associates with Sqh and directly binds the centralspindlin subunit Pav. We propose that during cytokinesis the reciprocal dependence between NMII and PI(4)P-GOLPH3 regulates centralspindlin stabilization and contractile ring structure at the cleavage site.

Results

Molecular cloning of the *Drosophila celibe* gene

The *celibe*[z2097] (*cbe*[z2097]) allele was identified during a cytological screen for mutants affecting cytokinesis in *Drosophila* spermatocytes (Giansanti et al., 2004). *cbe*[z2097] mutant males displayed multinucleate spermatids indicating defective meiotic cytokinesis (Giansanti et al., 2004). Complementation analysis with a series of chromosomal deletions uncovering the second chromosome revealed that *cbe*[z2097] complemented *Df(2R)BSC604* but failed to complement *Df(2R)BSC608* for both male sterility and the cytokinesis defects (Fig. 1B) indicating that it maps to a genomic interval that contains the *zipper* (*zip*) gene, encoding the *Drosophila* non-muscle myosin II heavy chain (Mansfield et al., 1996). The *zip* EMS induced alleles *zip*[1] (Young et al., 1993; Zhao et al., 1988) and *zip*[2] (Young et al., 1993; Zhao et al., 1988) failed to complement *cbe*[z2097] for male sterility and male meiotic failures indicating that *cbe*[z2097] is a mutant allele of *zip* (Fig. 1C,D*)*. DNA sequencing of the *cbe*[z2097] allele revealed two point mutations, relative to the reference sequence on Flybase, in the *zip* gene (Fig. 1E). The first mutation is located in a 45 residue N terminal extension of the Zip polypeptide (Mansfield et al. 1996), that is shared by three Zip isoforms (Flybase.org), resulting in the replacement of a threonine residue by proline (Fig. 1D). The second mutation is located within a highly conserved region common to all the Zip isoforms, resulting in the substitution of a conserved isoleucine into a phenylalanine (Fig. 1D). However, the threonine-to-proline substitution is not likely to be the cause of the mutant phenotype as the same substitution is also present in the original fly line prior to mutagenesis which does not exhibit sterility and spermatocyte cytokinesis failures (Zuker line, Koundakjian et al., 2004). The conserved isoleucine is adjacent to the IQ motif, which is required for binding of Zip protein to the RLC Spaghetti Squash (Sqh) (Fig. 1D,E; Trybus et al., 1994; Uehara et al., 2010). Western blot analysis from adult testis and larval brain extracts from *cbe*[z2097]/*Df(2R)BSC608 (cbe/Df)* mutants revealed reduced Zip protein levels, suggesting that that *cbe* mutation also affects the stability of Zip protein (Fig. S1A,B).

Contractile rings of *cbe* mutants fail to constrict.

To gain further insight into the cytokinesis phenotype of the *cbe/Df* mutants, dividing spermatocytes were stained for Zip protein (Fig. 2A). All the spermatocytes from both wild-type and *cbe/Df* mutant males, assembled Zip rings at the equatorial cortex during late anaphase-early telophase (Fig. 2A). However, in *cbe/Df* spermatocytes, localization of Zip protein at cell equator was greatly reduced and associated with thin rings. Strikingly in dividing spermatocytes from *cbe/Df* males the majority of Zip protein accumulated into cytoplasmic aggregates (Fig. 2A). Analysis of mid-late telophase revealed that 100% of wild-type spermatocytes displayed tight and constricted Zip rings (Fig. 2A). Conversely in *cbe/Df* mutant spermatocytes, fixed at mid-telophase, Zip protein formed unconstricted and fragmented rings and was enriched in large cytoplasmic aggregates (Fig. 2A). Immunofluorescence analysis revealed that the RLC fused to the green fluorescent protein Spaghetti Squash-GFP (Sqh-GFP, Royou et al., 2002) concentrated into an equatorial ring that co-localized with the Zip protein in wild-type telophase spermatocytes (Fig. 2B) but failed to accumulate in the cleavage furrow of *cbe/Df* telophases (Fig. 2B). Previous analyses failed to detect F-actin rings in *cbe* mutant spermatocytes (Giansanti et al. 2004). However, examination of fixed mutant spermatocytes with our improved F-actin staining protocol (Frappaolo et al., 2017a), revealed that *cbe/Df* mutant spermatocytes assemble F-actin rings that are substantially thinner than in wild type and fail to constrict (Fig. S2). Localization of Septins was also affected in *cbe* mutants. In wild-type and *cbe/Df* mutant spermatocytes at early telophase, the septin Sep1 accumulated in the cleavage furrow (Fig. S3). However, Septin rings failed to constrict and fragmented in mid-late telophases of *cbe/Df* mutants (Fig. S3).Immunofluorescence analysis revealed that wild-type function of Zip is also required for normal contractile ring constriction in larval brain neuroblasts. In wild-type dividing neuroblasts stained for tubulin and Zip, Zip protein localized to the basal cortex during early anaphase and concentrated at the furrow during early telophase (Fig. 3A). Immunostaining of *cbe/Df* mutant dividing neuroblasts revealed that Zip cortical localization is less robust than in wild type during both anaphase and telophase (Fig. 3B). Moreover *cbe/Df* mutant neuroblasts at late telophase fail to pinch the central spindle midzone during cytokinesis (Fig. 3A,B). Immunostaining of larval brains for tubulin and the contractile ring protein Anillin (Goldbach et al., 2010; Oegema et al., 2000) also revealed cytokinesis defects. Anillin accumulated to the cleavage furrow of both wild type and *cbe/Df* mutant neuroblasts during telophase (Fig. 3C,D). However, in 70% *cbe/Df* mutant neuroblasts at late telophase, the Anillin rings appeared large and unconstricted versus 0% in control (Fig. 3C,D).

***cbe/Df* mutant spermatocytes display defective GOLPH3 and centralspindlin localization at the cleavage site.**

We recently demonstrated that GOLPH3 protein accumulates at the cleavage furrow and is required for maintenance of NMII rings during cytokinesis (Sechi et al., 2014). Localization of GOLPH3 was abolished by *cbe* mutation. In wild-type dividing spermatocytes GOLPH3 protein accumulated at the equatorial site during telophase (Fig. 4). In contrast GOLPH3 protein was not detected at the cleavage site of *cbe/Df* mutant telophases (Fig. 4). Dividing spermatocytes from *cbe/Df* mutants also displayed defective central spindle structures (Figs. 2,4,5, S3). Our previous work showed that GOLPH3 function enables maintenance of centralspindlin complex at cell equator during cytokinesis (Sechi et al., 2014). In agreement with these data, localization of the RacGAP50C component of the centralspindlin complex (D'Avino et al., 2006) was affected in *cbe/Df* mutant dividing spermatocytes during telophase (Fig. 5A-D). In wild-type and *cbe/Df* mutant spermatocytes stained for tubulin and RacGAP50C, RacGAP50C started to accumulate at the peripheral and interior microtubules during mid-anaphase (Fig. 5A,B). In early telophase spermatocytes from wild type, RacGAP50C formed a tight equatorial band at the midzone of the central spindle, that constricted during mid- and late telophase (Fig. 5A). Conversely, early telophase spermatocytes from *cbe/Df* mutants displayed a faint localization of RacGAP50C at the interior and the peripheral microtubules (Fig. 5A). During later stages of *cbe/Df* mutant telophase, RacGAP50C either failed to accumulate, or was enriched at the interior microtubules with no appreciable concentration at the cortex (Fig. 5A).

Anillin is thought to act as molecular scaffold that links the plasma membrane with the contractile ring (D'Avino, 2009; Kechad et al., 2012; Liu et al., 2012; Takeda et al., 2013). Moreover, previous studies in *Drosophila* demonstrated that RacGAP50C interacts directly with Anillin and provides a link between the actomyosin ring and the peripheral microtubules (D'Avino et al., 2008; Gregory et al., 2008) We thus immunostained dividing *cbe/Df* spermatocytes for either tubulin and Anillin (Fig. S4) or Anillin and RacGAP50C (Fig. 5C,D). In dividing wild-type and *cbe/Df* spermatocytes stained for tubulin and Anillin, Anillin started to accumulate at the cell equator during early anaphase and formed a circumferential band at the equatorial cortex during early telophase (Fig. S4). Consistent with previous observations on *cbe* homozygous mutants (Giansanti et al., 2004) and unlike wild-type spermatocytes, *cbe/Df* spermatocytes stained at later stages of telophase displayed unconstricted Anillin rings (Fig. S4). In wild-type dividing spermatocytes stained for Anillin and RacGAP50C during mid-late telophase the RacGAP50C equatorial band was juxtaposed with the Anillin ring (Fig. 5C,D). Conversely in mid-telophase spermatocytes from *cbe/Df males*, the Anillin ring and the spindle-associated RacGAP50C appeared dissociated (Fig. 5C,D).

cbe mutation affects Zip/Sqh interaction in *Drosophila* testis extracts.

Since the *cbe* mutation substitutes a conserved isoleucine is adjacent to the IQ motif (Fig. 1D,E), we asked whether the *cbe^{z2097}* mutant allele could influence the assembly of the Zip-Sqh complex. Co-

immunoprecipitation (Co-IP) analysis from testis extracts indicated that *cbe* mutation impaired the interaction of Zip protein with Sqh (Fig. 6A) Our previous findings suggested that GOLPH3 interacts with Zip and other cytokinesis proteins in *Drosophila* (Sechi et al. 2014). Moreover recent work showed that Sqh protein binds to PI(4)P *in vitro* and mediates plasma membrane localization of PI(4)P in *Drosophila* neural stem cells (Koe et al., 2018). We then assessed whether GOLPH3 protein interacts with Sqh-GFP (Fig. 6A,B; Fig. S5). GST pull-down experiments showed that Sqh-GFP interacts with GOLPH3 (Fig. 6B). Co-IP experiments from adult testes indicated that GOLPH3 co-precipitated with Sqh-GFP (Fig. S5) and that the interaction partially depends on the Sqh-Zip complex (Fig. 6A)

Our previous work suggested that GOLPH3 associates with Pavarotti (Pav; Adams et al., 1998), the kinesin-like protein that works together with RacGAP50C in the centralspindlin complex (Sechi et al., 2014). Mislocalization of RacGAP50C at the cleavage site of *cbe* mutants led us to further investigate GOLPH3-Pav interaction. Pav-YFP (Szafer-Glusman et al., 2008) was immunoprecipitated for YFP and probed for GOLPH3 (Fig. 7A). To assess whether GOLPH3 could directly bind to Pav protein, we purified various Pav fragments (Bassi et al., 2013) tagged with glutathione S-transferase (GST) from bacteria and tested their ability to pull down 6XHis::GOLPH3 (Fig. 7B-D). These experiments suggested that GOLPH3 interacts with the Pav stalk and tail C-terminal domains (Fig. 7C-D). These data were confirmed using yeast two-hybrid assays (Fig. 7E).

Discussion

We have shown that *cbe^z2097* identified during a screen for male sterile mutations affecting spermatocyte cytokinesis, is a missense allele of *Drosophila zipper*. The *cbe^z2097* allele does not affect female fertility or fly viability in *cbe^z2097/Df, cbe/zip^1* and *cbe/zip^2* animals. The underlying cause of the different effects of the *cbe* mutation on female and male fertility may depend on sex specific regulatory mechanisms and different expression patterns of the non-muscle Myosin Zipper isoforms that remain to be clarified. In this context MYH10, the heavy chain of NMIIB, is required for meiotic cytokinesis in male but not in female mice (Yang et al., 2012).

Several studies have shown the requirement for the NMHC II Zip for cytokinesis in *Drosophila* cultured cells (Dean et. al., 2005; Echard et al., 2004; Eggert et al., 2004; Hickson et al., 2006; Straight et al., 2003, Straight et al. 2005). Analysis of cortical localization of truncated NMHC II proteins in *Drosophila* S2 cells has revealed that preassembled Myosin filaments accumulate to the equatorial cortex in the absence of Rho (Uehara et al., 2010). Here we have shown that *cbe* mutants carry a mutation in a conserved region of the Zip protein, which replaces an isoleucine residue adjacent to the RLC-binding IQ motif. The hydrophobic amino acid isoleucine is often involved in binding to hydrophobic ligands including lipids. We thus surmise that the substitution of isoleucine with the

aromatic amino acid phenylalanine might affect the interaction of NMHC II with the plasma membrane and the assembly of myosin thick filaments at the cleavage site. In agreement with this hypothesis, mammalian NMII proteins were found to bind to liposomes containing one or more acidic phospholipids but not to liposomes that contain 100% phosphatidylcoline (Liu et al., 2016). Liu and collaborators (Liu et al., 2016) showed that liposome binding of NMIIs to negatively charged liposomes, occurs predominantly through the interaction of the liposomes with the regulatory light chain (RLC) binding site of the heavy chain (HC) suggesting that membrane-bound monomers might associate with regulatory light chains and initiate polymerization of Myosin filaments. Remarkably the short sequence of the NMHC II involved in binding to anionic phospholipids contains a high percentage of hydrophobic amino acids (~55%) and basic amino acids (~24%) (Liu et al., 2016). Similarly, *Acanthamoeba* Myosin IC binds to acidic phospholipids *in vitro* through a short sequence of basic/hydrophobic amino acids, named the BH site, located in the non-helical tail (Brzeska et al. 2008). Moreover a BH site in the tail of *Dictyostelium* Myosin IB was shown to mediate binding to PI(4,5)P2 /PI(3,4,5)P3 enriched regions of the plasma membrane *in vivo* (Brzeska et al. 2012). Since PI(4,5)P2 is enriched at the cleavage furrow of dividing spermatocytes (Sechi et al. 2014; Wong et al. 2005), it is likely that wild type Zip protein might interact with this acidic phospholipid at the furrow plasma membrane.

A recent study showed that the RLC Sqh contributes to Phosphatidylinositol 4-Phosphate [PI(4)P] localization to the cortical plasma membrane of *Drosophila* neuroblasts indicating that a reciprocal dependence between Myosin II and plasma membrane phosphoinositides (Koe et al., 2018). Our findings demonstrate that *cbe* mutation impairs the association of Zip protein to the RLC Sqh. Despite the lack of Zip/Sqh interaction, *cbe* mutant spermatocytes display initial concentration of Zip protein in thin rings at the cleavage site of dividing cells. Recruitment of Sqh is abolished in *cbe* mutants leading to failure to assemble tight contractile rings and causing cytokinesis failures. These results are consistent with work from Beach and Egelhoff showing recruitment of mammalian NMHC II to the furrow independently RLC (Beach and Egelholff, 2009). Overall these data indicate that the mechanisms that concentrate NMHC II at the cleavage site do not require centralspindlin-mediated RLC-phosphorylation. However, Zip/Sqh interaction is required for formation of robust actomyosin rings and contractile ring constriction.

Our immunofluorescence analysis of *cbe* dividing spermatocytes showed that Zip/Myo protein concentrates in large cytoplasmic aggregates. Zip aggregates were also reported in embryos and egg chambers from which *sqh* was removed and might result from anomalous heavy chain interactions due to the exposure of the hydrophobic IQ motifs in the absence of binding to regulatory

light chains (Edwards and Kiehart, 1996; Franke et al., 2006; Jordan and Karess, 1997; Wheatley et al., 1995). Remarkably RLC-deficient Myosins have been shown to aggregate (Trybus et al., 1994).

One important conclusion from our study is the reciprocal dependence of GOLPH3 and NMII during the early events of cytokinesis. Our previous work demonstrated that GOLPH3 function during cytokinesis is intimately connected to its ability to bind to PI(4)P. GOLPH3 recruitment to the cleavage site depends on PI(4)P. Reciprocally, concentration of PI(4)P at the cleavage furrow requires wild type function of GOLPH3 (Sechi et al., 2014). Moreover, we demonstrated that GOLPH3 function is required to maintain centralspindlin at cell equator and stabilization of Myosin II and Septin rings at the cleavage furrow (Sechi et al., 2014). Based on our findings in this paper we propose a model whereby the coordinated function of NMII with GOLPH3 regulates centralspindlin stabilization at the cleavage furrow and contractile ring assembly. As depicted in Fig. 8, initial recruitment of Zip protein at the cleavage site does not require prior binding to Sqh. Robust actomyosin ring formation requires binding to Sqh protein which enables plasma membrane localization of GOLPH3 and presumably of PI(4)P at the cleavage site. Consistent with this model Sqh protein was shown to bind to PI(4)P *in vitro* which contributes to its membrane localization in neuroblasts (Koe et al., 2018). Our findings that *Drosophila* GOLPH3 binds to C-terminal domains of Pav suggest that GOLPH3 might regulate the association of centralspindlin with the plasma membrane during cytokinesis and stability of this complex at the invaginating membrane. Centralspindlin localization at the cleavage furrow is likely to be also stabilized by the interaction of RacGAP50C with PI(4)P and other polyanionic phosphoinositide lipids. In agreement with this model, Lekomtsev and coauthors (2012) reported that HsCyk4/MgcRacGAP interacts with PI(4)P and PI(4,5)P2 phosphoinositides at the furrow plasma membrane via its C1 domain. Moreover, data from Basant and coauthors (2015) in *C. elegans* showed that CYK-4-C1 domain enables association of centralspindlin complex oligomers with the plasma membrane to activate Rho A. In conclusion our study suggests that a close relationship between NMII filaments and PI(4)P-GOLPH3 may underlie centralspindlin stabilization and contractile ring constriction at the cleavage site. Since Anillin binds to Myosin and CYK-4/RacGAP50C (D'Avino et al., 2008; Gregory et al., 2008; Straight et al., 2005), it is possible that the Anillin-Zipper-Sqh-GOLPH3 module might function as a physical linker between the cleavage furrow and the central spindle during cytokinesis. Indeed, the spindle-associated RacGAP50C band loses its association with the Anillin-cortical ring in *cbe/Df* telophase spermatocytes. Because GOLPH3, Myosin II and Anillin have been all involved in tumor formation and progression (Nayden et al., 2020; Scott et al. 2009; Sechi et al., 2020; Wang et al., 2018), a minute dissection of their roles in the early events of cytokinesis may aid to identify new strategies to treat cancers.

Materials and Methods

Fly stocks

Flies were reared according to standard procedures at 25 °C. Oregon-R flies were used as wild-type controls unless otherwise specified. The cbe^{z2097} mutant strain was identified during a cytological screen of the Zuker's collection of male sterile mutants (Giansanti et al., 2004; Koundakjian et al., 2004). Flies expressing Pav-YFP were previously described (Szafer-Glusman et al, 2008). The chromosomal deficiencies *Df(2R)BSC604* and *Df(2R)BSC608*, the two alleles zip^1 (Zhao et al., 1988) and zip^2 (Young et al., 1993) and P(sqh-GFP.RLC) (Royou et al., 2002) were obtained from the Bloomington Drosophila Stock Center (Indiana University, Bloomington, IN).

Microscopy and histology

To quantify multinucleate spermatids, squashed live spermatid preparations were imaged on a Nikon Axioplan epifluorescence microscope equipped with a 40x phase-contrast objective. Cytological preparations for immunofluorescence analysis were made with brains and testes from third instar larvae. To visualize Sqh-GFP with Zip, or GOLPH3 with tubulin, larval testes were dissected in phosphate buffered saline (PBS), transferred to 5 µl of 4% methanol-free formaldehyde (Polysciences, Warrington, PA, USA) in PBS on a 20x20 coverslip (7 min) and gently squashed. Preparations were then immersed into liquid nitrogen and after coverslip removal with a razor blade, rinsed in PBS (2x5 min). For all other immunofluorescence experiments, preparations were fixed using 3.7% formaldehyde in PBS and then squashed in 60% acetic acid, as previously described in Szafer-Glusman et al. (2011). All samples were permeabilized and blocked in PBS (2x5 min) with 0.1% Triton X-100 and 3% BSA before immunofluorescence. Monoclonal antibodies were used to stain α-Tubulin (1:300; Sigma-Aldrich, T6199) and GFP (1:1000, 3E6, Thermofisher Scientific). Polyclonal antibodies were as follows: rabbit anti-Zip (1:500, gift of R. Karess, Paris Diderot University, Royou et al., 2002); rabbit anti-Sep1(1:30; gift of J. Pringle, Stanford University, CA, Fares et al., 1995; Field et al., 1996): rabbit anti-RacGAP50C (1:500; gift of D. M. Glover, University of Cambridge, D'Avino et al., 2006); rabbit anti-Cnn (1:300; gift of T. Megraw, Florida State University, Li et al., 1998), rabbit and mouse anti-Anillin (1:1000; Giansanti et al., 2015; Sechi et al., 2017), rabbit anti-GOLPH3 (G49139/77, 1:1000, Sechi et al., 2014). Secondary antibodies were: Alexa 555-conjugated anti-rabbit IgG (1:300, Life Technology) and FITC-conjugated anti-mouse IgG (1:30, Jackson ImmunoResearch). All incubations with primary antibodies (diluted in PBT containing 3% BSA) were performed overnight at 4°C. Incubations with secondary antibodies were performed at room temperature for 1h. After immunostaining, samples were rinsed in PBS and mounted in Vectashield mounting medium with DAPI (H-1800, Vector Laboratories). To stain F-actin with Rhodamine-Phalloidin (Invitrogen), larval testes were fixed in 4% methanol-free

formaldehyde (Polysciences, Warrington, PA, USA) in PBS as previously described (Frappaolo et al., 2017a). Images of testes stained for Sqh-GFP/Zip, were taken by an Axio Imager Z1 microscope (Carl Zeiss) equipped with an AxioCam HR cooled charge-coupled camera (Carl Zeiss). All the other images were captured with a charged-coupled device (CCD camera, Qimaging QICAM Mono Fast 1394 Cooled), connected to a Nikon Axioplan epifluorescence microscope equipped with an HBO 100-W mercury lamp and 40X and 100X objectives.

Molecular cloning

To identify the mutation in EMS-induced cbe^{z2097} allele, the genomic DNA corresponding to *zip* was amplified by PCR and sequenced on both strands (BMR research service). DNA sequences from cbe^{z2097} individuals were compared to sequences of the original Zuker-background chromosome to confirm the point mutation. The pET Directional TOPO Expression kit (Thermofisher Scientific) was used to obtain 6XHis::GOLPH3 (Sechi et al., 2017).

Co-Immunoprecipitation

Co-IP experiments were performed from testes expressing either Sqh-GFP (Fig. 6) or Pav-YFP (Fig. 7) using the procedure described previously (Belloni et al., 2012). 200 adult testes expressing Sqh-GFP, for each genotype, were homogenized in 500 µl of Lysis buffer (10 mM Tris–HCl pH 7.5, 150 mM NaCl, 0.5 mM EDTA, 0.5% NP40, 1 mM PMSF, 1× protease inhibitor cocktail) for 40 min on ice using a Dounce homogenizer. Lysates were clarified by centrifugation and protein concentration was quantified using NanoDrop 2000c Spectrophotometer (Thermo Scientific). 2% of each lysate was retained as the "input", the remainder was precleared with control agarose beads (Chromotek, Bab-20). Co-IP was performed using the GFP trap-A or control binding beads purchased from ChromoTek (Planegg-Martinsried), following the protocol that was previously described (Belloni et al., 2012).

Western Blotting

Immunoblotting analysis of Zip protein was performed from protein extracts of either adult testes or larval brains. 40 testes or 20 brains from males of each genotype, were homogenized on ice in 100 µl of Lysis buffer (10 mM Tris-HCl pH 7.5, 150 mM NaCl, 0.5 mM EDTA, 0.5% NP-40, 1× Protease Inhibitor Cocktail) using a Dounce homogenizer. Cell lysates were cleared by centrifugation and protein concentration of supernatants was determined using the Qubit 4 Fluorometer (Invitrogen). Equal amounts of protein were analyzed by SDS-PAGE and Western blotting. Samples were separated on Bolt Mini Gels (Novex) and blotted to PVDF membranes (Bio-Rad). Membranes were blocked in Tris-buffered saline (Sigma-Aldrich) with 0,05% Tween-20 (TBS-T) containing 5% nonfat dry milk (Bio-Rad; Blotting GradeBlocker) for 1 h at room temperature followed by incubation with primary and secondary antibodies diluted in TBS-T. Primary antibodies used for

immunoblotting were as follows: mouse anti-GOLPH3 S11047/1/56 (1:2500; Sechi et al., 2014), rabbit anti-GFP (1:1000; TP401, Torrey Pines), Rabbit anti-Zip (1:2000, gift from R.E. Karess), rabbit anti-RacGAP50C (1:500; gift of D.M. Glover, University of Cambridge, D'Avino et al., 2006); mouse α-Tubulin (1:300; Sigma-Aldrich, T6199), mouse anti-6XHis (1:100, Invitrogen). HRP-conjugated secondary antibodies were as follows: Goat anti-Mouse IgG (H+L) (Pierce, N.31431) and Goat anti-Rabbit IgG (H+L) (Pierce, N.31466). Secondary antibodies were used at 1:5000. After incubation with the antibodies, blots were washed (3X5 min) in TBS-T (20 mM Tris–HCl pH 7.5, 150 mM NaCl, 0.05% Tween 20). Blots were imaged using ECL (Cyanagen, XLS100) and signals revealed with the ChemiDoc XRS imager (BioRad).

Protein expression and GST pull-down

The constructs expressing GST::Pav proteins were a kind gift from PP. D'Avino (University of Cambridge, Bassi et al., 2013). GST, GST::GOLPH3 and the GST::Pav proteins (GST::Pav$^{1-460}$, GST::Pav$^{461-685}$, GST::Pav$^{461-887}$, GST::Pav$^{686-887}$), were expressed in bacteria and purified using Glutathione-Sepharose 4B beads (GE Healthcare) following the manufacturer's instructions as described in Giansanti et al., 2015 and Sechi et al., 2017. 6XHis::GOLPH3 was expressed in bacteria and purified using cOmplete His-Tag Purification Resin (Roche). Direct interaction between 6XHis-GOLPH3 and GST-Pav proteins was carried out using the protocol described previously (Sechi et al., 2017). The GST pull-down experiment in Fig. 6 was performed with testis lysates using the procedure described in Frappaolo et al., 2017b. At least 200 adult testes were homogenized for 40 minutes on ice in 500 µl of Lysis buffer (25mM Tris-HCl pH 7.4, 150mM NaCl, 0,5% NP-40, 1mM EDTA) with the addition of Protease and Phosphatase inhibitors cocktails (Roche), using a Dounce homogenizer. GST pull-down was performed by incubating testis lysates with either GST or GST-GOLPH3 (at the appropriate concentration) bound to Glutathione-Sepharose 4B beads (GE healthcare Life sciences), with gentle rotation, at 4°C for two hours. After rinsing in "wash buffer" (25mM Tris-HCl pH 7.4, 150mM NaCl, 1% NP-40, 1mM EDTA, Protease and phosphatase inhibitors), for three times, the beads were boiled in SDS sample buffer, and separated by SDS-PAGE. The bound proteins were analyzed by Western Blotting. Before immunoblotting, PVDF membranes were stained with Ponceau (Sigma-Aldrich).

Yeast two-hybrid assay

The assay was performed as previously described (Frappaolo et al., 2017b) using the B42/lexA system with strain EGY48 (Mata his3 ura3 trp1 6lexAOP-LEU2; lexAOP-lacZ reporter on plasmid pSH18-34) as the host strain (Cassani et al., 2013). The host strain was co-transformed with various combinations of bait (pEG202) and prey (pJG4-5) plasmids carrying Pav fragments and GOLPH3 respectively. To assess two-hybrid interaction, the strains were spotted on 5-bromo-4-chloro-3-

indolyl-β-d-galactopyranoside (X-GAL) selective synthetic plates containing either raffinose (RAFF, prey not induced) or 2% galactose (GAL, prey expressed), as described by Cassani et al. (2013). To quantify the yeast two-hybrid results, a β-galactosidase assay was performed. Strains were first grown in a selective medium containing galactose, then cells were collected and protein extracts prepared in order to test β-galactosidase enzyme activity using o-nitrophenyl-d-galactoside (ONPG) as a substrate, as described by Polevoy et al. (2009). For each sample, five independent transformants were used and the assays were performed in duplicate to calculate average β-galactosidase units and standard error.

Statistical analysis

For all the immunofluorescence, differences between wild type and mutant cells were examined for statistical significance using Fisher's exact test with Prism 8 (Graphpad). Quantification of the density of Western blot bands using Image J (open source image processing program). Data are expressed as fold changes compared to control. All data represent the mean ± s.d. from three independent experiments. Unpaired Student's t-test analysis was performed with *P < 0.05, **P< 0.01, ***P <0.0001 and ns = not significant. The representative results, from at least three independent experiments were analyzed using unpaired Student's t-test with Prism 8 (Graphpad). For yeast two-hybrid experiments, differences between each group were examined for statistical significance using the Mann–Whitney U test using Prism 8 (Graphpad). P<0.05 was considered statistically significant.

References

Adams, R. R., Tavares, A. A., Salzberg, A., Bellen, H. J. and Glover, D. M. (1998). Pavarotti Encodes a Kinesin-Like Protein Required to Organize the Central Spindle and Contractile Ring for Cytokinesis. *Genes Dev*. **12**, 1483-1494. DOI: 10.1101/gad.12.10.1483

Basant, A., Lekomtsev, S., Tse, Y. C., Zhang, D., Longhini, K. M., Petronczki, M. and Glotzer, M. (2015). Aurora B Kinase Promotes Cytokinesis by Inducing Centralspindlin Oligomers That Associate With the Plasma Membrane. *Dev. Cell.* **33**, 204-215. DOI: 10.1016/j.devcel.2015.03.015

Bassi, Z. I., Audusseau, M., Riparbelli, M. G., Callaini, G. and D'Avino, P. P. (2013). Citron Kinase Controls a Molecular Network Required for Midbody Formation in Cytokinesis. *Proc. Natl. Acad. Sci.* U S A. **110**, 9782-9787. DOI: 10.1073/pnas.1301328110

Beach, J. R. and Egelhoff, T.T. (2009). Myosin II Recruitment during Cytokinesis Independent of Centralspindlin-mediated Phosphorylation. *J. Biol. Chem.* **284**, 27377–27383. DOI: 10.1074/jbc.M109.028316

Belloni, G., Sechi, S., Riparbelli, M. G., Fuller, M. T., Callaini, G. and Giansanti, M. G. (2012). Mutations in Cog7 affect Golgi structure, meiotic cytokinesis and sperm development during Drosophila spermatogenesis. *J. Cell Sci.* **125**, 5441-5452. DOI: 10.1242/jcs.108878

Brzeska, H., Hwang, K. J. and Korn, E. D. (2008). Acanthamoeba Myosin IC colocalizes with phosphatidylinositol 4,5-bisphosphate at the plasma membrane due to the High concentration of negative charge. *J. Biol. Chem.* **283**, 32014–32023. DOI: 10.1074/jbc.M804828200

Brzeska, H., Guag, J., Preston, G. M., Titus, M. A. and Korn, E. D. (2012). Molecular basis of dynamic relocalization of Dictyostelium Myosin IB. *J. Biol. Chem.* **287**, 14923–14936. DOI: 10.1074/jbc.M111.318667

Cassani, C., Raspelli, E., Santo, N., Chiroli, E., Lucchini, G. and Fraschini, R. (2013). Saccharomyces Cerevisiae Dma Proteins Participate in Cytokinesis by Controlling Two Different Pathways. *Cell Cycle.* **12**, 2794-2808. DOI: 10.4161/cc.25869

D'Avino, P. P., Takeda, T., Capalbo, L., Zhang, W., Lilley, K. S., Laue, E. D. and Glover, D. M. (2008). Interaction between Anillin and RacGAP50C connects the actomyosin contractile ring with spindle microtubules at the cell division site. *J Cell Sci*. **121**, 1151-1158. DOI: 10.1242/jcs.026716

D'Avino, P.P. (2009) How to scaffold the contractile ring for a safe cytokinesis - lessons from Anillin-related proteins. *J. Cell Sci.* **122**, 1071-1079. DOI: 10.1242/jcs.034785.

D'Avino, P. P., Savoian, M. S., Capalbo, L. and Glover, D. M. (2006). RacGAP50C Is Sufficient to Signal Cleavage Furrow Formation During Cytokinesis. *J. Cell. Sci.* **119**, 4402-4408. DOI: 10.1242/jcs.03210

D'Avino, P. P., Giansanti M. G. and Petronczki, M. (2015). Cytokinesis in Animal Cells. *Cold Spring Harb. Perspect. Biol.* **7**, a015834. DOI: 10.1101/cshperspect.a015834

De Lozanne A. and Spudich, J. A. (1987). Disruption of the Dictyostelium Myosin Heavy Chain Gene by Homologous Recombination. *Science.* **236**, 1086-1091. DOI: 10.1126/science.3576222

Dean, S. O., Rogers, S. L., Stuurman, N., Vale, R. D. and Spudich, J. A. (2005). Distinct Pathways Control Recruitment and Maintenance of Myosin II at the Cleavage Furrow During Cytokinesis. *Proc. Natl. Acad. Sci. U S A.* **102**, 13473-13478. DOI: 10.1073/pnas.0506810102

Echard, A., Hickson, G. R., Foley, E. and O'Farrell, P. H. (2004). Terminal cytokinesis events uncovered after an RNAi screen. *Curr. Biol.* **14,** 1685-1693. DOI: 10.1016/j.cub.2004.08.063

Eda, M., Yonemura, S., Kato, T., Watanabe, N., Ishizaki, T., Madaule, P. and Narumiya S. (2001). Rho-dependent Transfer of Citron-kinase to the Cleavage Furrow of Dividing Cells. *J. Cell Sci.* **114**, 3273-3284

Edwards, K. A. and Kiehart, D. P. (1996). Drosophila Nonmuscle Myosin II Has Multiple Essential Roles in Imaginal Disc and Egg Chamber Morphogenesis. *Development.* **122**, 1499-1511

Eggert, U. S., Kiger, A. A., Richter, C., Perlman, Z. E., Perrimon, N., Mitchison T. J. and Field, C. M. (2004). Parallel Chemical Genetic and Genome-Wide RNAi Screens Identify Cytokinesis Inhibitors and Targets. *PLoS Biol.* **2**, e379. DOI: 10.1371/journal.pbio.0020379

Fares, H., Peifer, M. and Pringle, J. R. (1995). Localization and Possible Functions of Drosophila Septins. *Mol. Biol. Cell.* **2**, 1843-1859. DOI: 10.1091/mbc.6.12.1843

Field, C. M., al-Awar, O., Rosenblatt, J., Wong, M. L., Alberts, B. and Mitchison T. J. (1996). A Purified Drosophila Septin Complex Forms Filaments and Exhibits GTPase Activity. *J. Cell Biol.* **133**, 605-616. DOI: 10.1083/jcb.133.3.605

Franke, J. D., Boury, A. L., Gerald, N. J. and Kiehart, D. P. (2006). Native Nonmuscle Myosin II Stability and Light Chain Binding in Drosophila Melanogaster. *Cell. Motil. Cytoskeleton.* **63**, 604-622. DOI: 10.1002/cm.20148

Frappaolo, A., Sechi, S., Belloni, G., Piergentili, R. and Giansanti, M. G. (2017a). Visualization of cleavage furrow proteins in fixed dividing spermatocytes. *Methods Cell Biol.* **137**, 85-103. DOI: 10.1016/bs.mcb.2016.03.035

Frappaolo, A., Sechi, S., Kumagai, T., Robinson, S., Fraschini, R., Karimpour-Ghahnavieh, A., Belloni, G., Piergentili, R., Tiemeyer, K.H., Tiemeyer, M. et al. (2017b). COG7 Deficiency in Drosophila Generates Multifaceted Developmental, Behavioral and Protein Glycosylation Phenotypes. *J. Cell Sci.* **130**, 3637-3649. DOI: 10.1242/jcs.209049

Giansanti, M. G. and Fuller, M. T. (2012). What Drosophila spermatocytes tell us about the mechanisms underlying cytokinesis. *Cytoskeleton (Hoboken)* **69,** 869–881. DOI: 10.1002/cm.21063

Giansanti, M. G., Farkas, R. M., Bonaccorsi, S., Lindsley, D. L., Wakimoto, B. T., Fuller, M. T. and Gatti, M. (2004). Genetic Dissection of Meiotic Cytokinesis in Drosophila Males. *Mol. Biol. Cell.* **15**, 2509–2522. DOI: 10.1091/mbc.e03-08-0603

Giansanti, M. G., Vanderleest, T. E., Jewett, C. E., Sechi, S., Frappaolo, A., Fabian, L., Robinett, C. C., Brill, J. A., Loerke, D., Fuller, M. T. et al. (2015). Exocyst-Dependent Membrane Addition Is Required for Anaphase Cell Elongation and Cytokinesis in Drosophila. *PLoS Genet.* **11**, e1005632. DOI: 10.1371/journal.pgen.1005632

Gregory, S. L., Ebrahimi, S., Milverton, J., Jones, W. M., Bejsovec, A. and Saint, R. (2008). Cell division requires a direct link between microtubule-bound RacGAP and Anillin in the contractile ring. *Curr. Biol.* **18**, 25-29. DOI: 10.1016/j.cub.2007.11.050

Goldbach, P., Wong, R., Beise, N., Sarpal, R., Trimble W. S. and Brill, J. A. (2010). Stabilization of the Actomyosin Ring Enables Spermatocyte Cytokinesis in Drosophila. *Mol. Biol. Cell.* **21,** 1482–1493. DOI: 10.1091/mbc.e09-08-0714

Hickson, G. R. X., Echard A., and O'Farrell P. H. (2006). Rho-kinase Controls Cell Shape Changes During Cytokinesis. *Curr. Biol.* **16**, 359-370. DOI: 10.1016/j.cub.2005.12.043

Ishizaki, T., Maekawa, M., Fujisawa, K., Okawa, K., Iwamatsu, A., Fujita, A., Watanabe, N., Saito, Y., Kakizuka, A., Morii, N. et al. (1996). The small GTP-binding protein Rho binds to and activates a 160 kDa Ser/Thr protein kinase homologous to myotonic dystrophy kinase. *EMBO J.* **15**, 1885–1893. DOI: 10.1002/j.1460-2075.1996.tb00539.x

Jordan, P. and Karess, R. (1997). Myosin Light Chain-Activating Phosphorylation Sites Are Required for Oogenesis in Drosophila. *J. Cell Biol.* **139**, 1805-1819. DOI: 10.1083/jcb.139.7.1805

Kamijo, K., Ohara, N., Abe, M., Uchimura, T., Hosoya, H., Lee, J. S. and Miki, T. (2006). Dissecting the Role of Rho-mediated Signaling in Contractile Ring Formation. *Mol. Biol. Cell.* **17**, 43–55. DOI: 10.1091/mbc.e05-06-0569

Kechad, A., Jananji, S., Ruella, Y. and Hickson, G. R. (2012). Anillin acts as a bifunctional linker coordinating midbody ring biogenesis during cytokinesis. *Curr. Biol.* **22**, 197-203. DOI: 10.1016/j.cub.2011.11.062.

Ketchum, A. S., Stewart, C. T., Stewart, M. and Kiehart, D. P. (1990). Complete Sequence of the Drosophila Nonmuscle Myosin Heavy-Chain Transcript: Conserved Sequences in the Myosin Tail and Differential Splicing in the 5' Untranslated Sequence. *Proc. Natl. Acad. Sci.* U S A. **87**, 6316-6320. DOI: 10.1073/pnas.87.16.6316

Kiehart, D. P., Lutz, M. S., Chan, D., Ketchum, A. S., Laymon, R. A., Nguyen, B. and Goldstein, L. S. (1989). Identification of the gene for fly non-muscle myosin heavy chain: Drosophila myosin heavy chains are encoded by a gene family. *EMBO J.* **8**, 913-922. DOI: 10.1002/j.1460-2075.1989.tb03452.x

Koe, C. T., Tan, Y. S., Lönnfors, M., Hur, S. K., Low, C. S. L., Zhang, Y., Kanchanawong, P., Bankaitis, V. A. and Wang, H. (2018). Vibrator and PI4KIIIα govern neuroblast polarity by anchoring non-muscle myosin II. *eLife.* **7**, e33555. DOI: 10.7554/eLife.33555

Koundakjian, E. J., Cowan, D. M., Hardy, R. W. and Becker, A. H. (2004). The Zuker collection: a resource for the analysis of autosomal gene function in Drosophila melanogaster. *Genetics.* **167**, 203–206. DOI: 10.1534/genetics.167.1.203

Lekomtsev, S., Su, K. C., Pye, V. E., Blight, K., Sundaramoorthy, S., Takaki, T., Collinson, L. M., Cherepanov, P., Divecha, N. and Petronczki, M. (2012). Centralspindlin Links the Mitotic Spindle to the Plasma Membrane During Cytokinesis. *Nature.* **492**, 276-279. DOI: 10.1038/nature11773

Li, K., Xu, E. Y., Cecil, J. K., Turner, F. R., Megraw, T. L. and Kaufman T. C. (1998). Drosophila Centrosomin Protein is Required for Male Meiosis and Assembly of the Flagellar Axoneme. *J. Cell Biol.* **141**, 455–467. DOI: 10.1083/jcb.141.2.455

Liu, J., Fairn, G.D., Ceccarelli, D.F., Sicheri, F. and Wilde, A. (2012). Cleavage furrow organization requires PIP(2)-mediated recruitment of anillin. *Curr. Biol.* **22**, 64-69. DOI: 10.1016/j.cub.2011.11.040

Liu, X., Shu, S., Billington, N., Williamson, C. D., Yu, S., Brzeska, H., Donaldson, J. G., Sellers J. R. and Korn, E. D. (2016). Mammalian Non muscle Myosin II Binds to Anionic Phospholipids With Concomitant Dissociation of the Regulatory Light Chain. *J. Biol. Chem.* **291**, 24828-24837. DOI: 10.1074/jbc.M116.739185

Ma, X., Kovács, M., Conti, M. A., Wang, A., Zhang, Y., Sellers, J. R. and Adelstein, R. S. (2012). Nonmuscle myosin II exerts tension but does not translocate actin in vertebrate cytokinesis. *Proc. Natl. Acad. Sci. U S A.* **109**, 4509-4514. DOI: 10.1073/pnas.1116268109

Mabuchi, I. and Okuno, M. (1977). The effect of myosin antibody on the division of starfish blastomeres. *J. Cell Biol.* **74,** 251–263. DOI: 10.1083/jcb.74.1.251

Mansfield, G. S., Al-Shirawi, D. Y., Ketchum, A. S., Newbern C. E. and Kiehart D. P. (1996). Molecular Organization and Alternative Splicing in zipper, the Gene that Encodes the Drosophila Non-muscle Myosin II Heavy Chain. *J. Mol. Biol.* **255,** 98-109. DOI: 10.1006/jmbi.1996.0009

Matsumura, F., Yamakita, Y. and Yamashiro, S. (2011). Myosin light chain kinases and phosphatase in mitosis and cytokinesis. *Arch. Biochem. Biophys.* **510**, 76–82. DOI: 10.1016/j.abb.2011.03.002

Murakami, N., Kotula, L. and Hwang, Y. W. (2000). Two Distinct Mechanisms for Regulation of Non muscle Myosin Assembly via the Heavy Chain: Phosphorylation for MIIB and Mts 1 Binding for MIIA. *Biochemistry.* **39**, 11441-11451. DOI: 10.1021/bi000347e

Naydenov, N., Koblinski, J. and Ivanov A. (2020). Anillin is an emerging regulator of tumorigenesis, acting as a cortical cytoskeletal scaffold and a nuclear modulator of cancer cell differentiation. *Cell Mol Life Sci.* DOI: 10.1007/s00018-020-03605-9

Nishimura, Y. and Yonemura, S. (2006). Centralspindlin regulates ECT2 and RhoA accumulation at the equatorial cortex during cytokinesis. *J. Cell Sci.* **119**, 104-114. DOI: 10.1242/jcs.02737

Oegema, K., Savoian, M. S., Mitchison, T. J. and Field, C. M. (2000). Functional Analysis of a Human Homologue of the Drosophila Actin Binding Protein Anillin Suggests a Role in Cytokinesis. *J. Cell Biol.* **150**, 539–552. DOI: 10.1083/jcb.150.3.539

Osório, D.S., Chan, F.Y., Saramago, J., Leite, J., Silva, A. M., Sobral, A. F., Gassmann, R. and Carvalho, A. X. (2019). Crosslinking activity of non-muscle myosin II is not sufficient for embryonic cytokinesis in C. elegans. *Development.* **146**, dev179150. DOI: 10.1242/dev.179150

Piekny, A., Werner, M. and Glotzer, M. (2005). Cytokinesis: welcome to the Rho zone. *Trends Cell Biol.* **15**, 651-658. DOI: 10.1016/j.tcb.2005.10.006

Polevoy, G., Wei, H.-C., Wong, R., Szentpetery, Z, Kim, Y. J., Goldbach, P., Steinbach, S. K., Balla, T. and Brill, J. A. (2009). Dual Roles for the Drosophila PI 4-kinase Four Wheel Drive in Localizing Rab11 During Cytokinesis. *J. Cell Biol.* **187**, 847-858. DOI: 10.1083/jcb.200908107

Ronen D. and Ravid, S. (2009). Myosin II Tailpiece Determines Its Paracrystal Structure, Filament Assembly Properties, and Cellular Localization. *J. Biol. Chem.* **284**, 24948-24957. DOI: 10.1074/jbc.M109.023754

Royou, A., Sullivan, W. and Karess, R. (2002). Cortical Recruitment of Non muscle Myosin II in Early Syncytial Drosophila Embryos: Its Role in Nuclear Axial Expansion and Its Regulation by Cdc2 Activity. *J. Cell Biol.* **158**, 127-137. DOI: 10.1083/jcb.200203148

Scott, K. L, Kabbarah, O., Liang, M. C., Ivanova, E., Anagnostou, V., Wu, J., Dhakal S, Wu M, Chen S, Feinberg T, et al. (2009). GOLPH3 modulates mTOR signalling and rapamycin sensitivity in cancer. *Nature.* **459**, 1085-1090. DOI: 10.1038/nature08109

Sechi, S., Colotti, G., Belloni, G., Mattei, V., Frappaolo, A., Raffa, G. D., Fuller, M. T. and Giansanti, M. G. (2014). GOLPH3 Is Essential for Contractile Ring Formation and Rab11 Localization to the Cleavage Site During Cytokinesis in Drosophila Melanogaster. *PLoS Genet.* **10**, e1004305. DOI: 10.1371/journal.pgen.1004305

Sechi, S., Frappaolo, A., Fraschini, R., Capalbo, L., Gottardo, M., Belloni, G., Glover, D. M., Wainman, A. and Giansanti, M. G. (2017). Rab1 Interacts with GOLPH3 and Controls Golgi Structure and Contractile Ring Constriction During Cytokinesis in Drosophila Melanogaster. *Open Biol.* **7**, 160257. DOI: 10.1098/rsob.160257

Sechi, S, Frappaolo, A., Karimpour-Ghahnavieh, A., Piergentili, R. and Giansanti, M. G. (2020). Oncogenic roles of GOLPH3 in the Physiopathology of cancer. *Int. J. Mol. Sci.* **21**, 933. DOI: 10.3390/ijms21030933

Shutova, M. S. and Svitkina, T. M. (2018). Mammalian Nonmuscle Myosin II Comes in Three Flavors. *Biochem. Biophys. Res. Commun.* **506**, 394-402. DOI: 10.1016/j.bbrc.2018.03.103

Somers, W.G. and Saint, R. (2003). A RhoGEF and Rho Family GTPase-Activating Protein Complex Links the Contractile Ring to Cortical Microtubules at the Onset of Cytokinesis. *Dev. Cell.* **4**, 29–39. DOI: 10.1016/s1534-5807(02)00402-1

Straight, A. F., Cheung, A., Limouze, J., Chen, I., Westwood, N. J., Sellers, J. R. and Mitchison T. J. (2003). Dissecting Temporal and Spatial Control of Cytokinesis With a Myosin II Inhibitor. *Science*. **299**, 1743-1747. DOI: 10.1126/science.1081412

Straight, A. F., Field, C. M. and Mitchison, T. J. (2005). Anillin Binds Nonmuscle Myosin II and Regulates the Contractile Ring. *Mol. Biol. Cell.* **16**, 193-201. DOI: 10.1091/mbc.e04-08-0758

Szafer-Glusman, E., Giansanti, M. G., Nishihama, R., Bolival, B., Pringle, J., Gatti, M. and Fuller, M. T. (2008). A Role for Very-Long-Chain Fatty Acids in Furrow Ingression During Cytokinesis in Drosophila Spermatocytes. *Curr. Biol.* **18**, 1426-1431. DOI: 10.1016/j.cub.2008.08.061

Szafer-Glusman, E., Fuller, M. T. and Giansanti, M. G. (2011). Role of Survivin in cytokinesis revealed by a separation-of-function allele. *Mol. Biol. Cell*. **22**, 3779-3790. DOI: 10.1091/mbc.E11-06-0569

Takeda, T., Robinson, I. M., Savoian, M. M., Griffiths, J. R., Whetton, A. D., McMahon, H. T. and Glover, D. M. (2013). Drosophila F-BAR protein Syndapin contributes to coupling the plasma membrane and contractile ring in cytokinesis. *Open Biol.* **3**, 130081. DOI: 10.1098/rsob.130081

Trybus, K. M., Waller, G. S. and Chatman, T. A. (1994). Coupling of ATPase Activity and Motility in Smooth Muscle Myosin Is Mediated by the Regulatory Light Chain. *J. Cell Biol.* **124**, 963-969. DOI: 10.1083/jcb.124.6.963

Uehara, R., Goshima, G., Mabuchi, I., Vale, R. D., Spudich, J. A. and Griffis, E.R. (2010). Determinants of Myosin II Cortical Localization During Cytokinesis. *Curr. Biol.* **20**, 1080-1085. DOI: 10.1016/j.cub.2010.04.058

Vale, R.D., Spudich, J. A. and Griffis, E. R. (2009). Dynamics of myosin, microtubules, and Kinesin-6 at the cortex during cytokinesis in Drosophila S2 cells. *J. Cell Biol.* **186**, 727–738. DOI: 10.1083/jcb.200902083

Vicente-Manzanares, M., Ma, X., Adelstein, R. S. and Horwitz, A. R. (2009). Non-muscle myosin II takes centre stage in cell adhesion and migration. *Nat. Rev. Mol. Cell Biol.* **10,** 778–790. DOI: 10.1038/nrm2786

Wang, K., Wloka, C. and Bi, E. (2019). Non-muscle Myosin-II Is Required for the Generation of a Constriction Site for Subsequent Abscission. *iScience.* **13**, 69–81. DOI: 10.1016/j.isci.2019.02.010

Wang, Y., Yang, Q., Cheng, Y., Gao, M., Kuang, L. and Wang, C. (2018). Myosin Heavy Chain 10 (MYH10) Gene Silencing Reduces Cell Migration and Invasion in the Glioma Cell Lines U251, T98G, and SHG44 by Inhibiting the Wnt/β-Catenin Pathway. *Med Sci Monit.* **24**, 9110–9119. DOI: 10.12659/MSM.911523

Wheatley, S., Kulkarni, S. and Karess, R. (1995). Drosophila Nonmuscle Myosin II Is Required for Rapid Cytoplasmic Transport During Oogenesis and for Axial Nuclear Migration in Early Embryos. *Development.* **121**, 1937-1946.

Wong, R., Hadjiyanni, I., Wei, H.-C., Polevoy, G., McBride, R., Sem, K.-P., Brill, J. A. (2005). PIP2 hydrolysis and calcium release are required for cytokinesis in Drosophila spermatocytes. *Curr. Biol.* **15**, 1401-1406. DOI: 10.1016/j.cub.2005.06.060

Yamashiro, S., Totsukawa, G., Yamakita, Y., Sasaki, Y., Madaule, P., Ishizaki, T., Narumiya, S. and Matsumura, F. (2003). Citron Kinase, a Rho-dependent Kinase, Induces Di-phosphorylation of Regulatory Light Chain of Myosin II. *Mol. Biol. Cell.* **14**, 1745–1756. DOI: 10.1091/mbc.e02-07-0427

Yang, F., Wei, Q., Adelstein, R. S. and Wanga P. J. (2012). Non-muscle myosin IIB is essential for cytokinesis during male meiotic cell divisions. *Dev Biol*. **15**, 356–361. DOI: 10.1016/j.ydbio.2012.07.011

Young, P. E., Richman, A. M., Ketchum, A. S. and Kiehart, D. P. (1993). Morphogenesis in Drosophila Requires Nonmuscle Myosin Heavy Chain Function. *Genes Dev*. **7**, 29-41. DOI: 10.1101/gad.7.1.29

Yüce, Ö., Piekny, A. and Glotzer, M. (2005). An ECT2–centralspindlin complex regulates the localization and function of RhoA. *J. Cell Biol.* **170**, 571–582. DOI: 10.1083/jcb.200501097

Zhao, D. B., Côté, S., Jähnig, F., Haller, J. and Jäckle, H. (1988). Zipper Encodes a Putative Integral Membrane Protein Required for Normal Axon Patterning During Drosophila Neurogenesis. *EMBO J.* **7**, 1115-1119. DOI: 10.1002/j.1460-2075.1988.tb02920.x

Zhao, W. M. and Fang, G. (2005). MgcRacGAP Controls the Assembly of the Contractile Ring and the Initiation of Cytokinesis. *Proc. Natl. Acad. Sci. U S A*. **102**, 13158-13163. DOI: 10.1073/pnas.0504145102
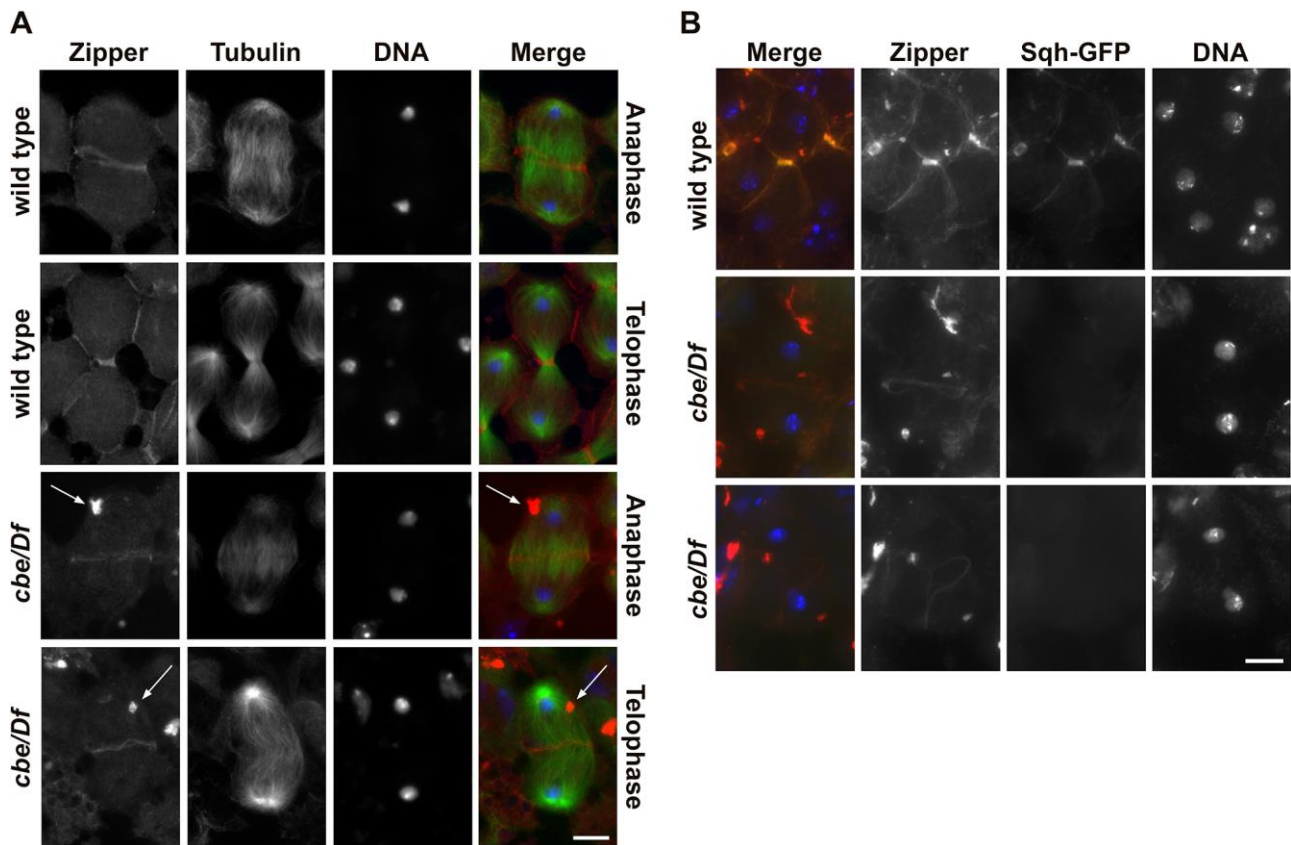
Figures

Fig. 1 cbe is a missense allele of the _zip_ gene. (A) Schematic depicting the subunits and the domain structure of non-muscle Myosin II. (B) Multinucleate onion stage spermatids due to cytokinesis failure during meiosis in cbe^{z2097} mutant males. (Nu) nucleus; (Nk) nebenkern (mitochondrial derivative). Scale Bar, 10μm. (C) Frequencies of spermatids containing 1 or more than 1 nucleus per Nk, in control Oregon-R males and cbe^{z2097} mutant males. Graph shows percentage ±s.d. Spermatids were examined from testes of at least 10 males per each genotype. Statistically significant differences are ***p<0.0001 (Fisher's exact test). (D) Schematic showing the domain organization of Zip protein and the amino acids mutated in cbe^{z2097}: permissive substitution of threonine (T) by proline (P), that is also present in the background chromosome; substitution of phenylalanine (F) for wild-type isoleucine (I) that underlies the _cbe_ phenotype. (E) Alignment of a portion of _Drosophila_ Zip protein with NMHC II proteins from different species.; (*) fully conserved residue; (:) conservation between groups of strongly similar properties. Arrow points to the amino acid mutated in _cbe_. Line indicates the last portion of the IQ motif (ScanProsite) with respect to the amino acid mutated in _cbe_.

Fig. 2 The *cbe* mutation affects NMII distribution at the cleavage site. (A) Wild-type and *cbe^{z2097}/Df(2R)BSC608 (cbe/Df)* mutant spermatocytes during late anaphase and mid-late telophase, stained for tubulin (green), DNA (blue) and Zip (red); N=40 wild-type and *cbe/Df* late-anaphase spermatocytes; N=60 wild-type and *cbe/Df* mid-late spermatocytes; randomly selected from images taken in five experiments. Arrows point to cytoplasmic aggregates containing Zip protein. (B) Wild-type and *cbe^{z2097}/Df(2R)BSC608 (cbe/Df)* mutant spermatocytes during late telophase, stained for Sqh (green), DNA (blue) and Zip (red). N= 40 wild-type and *cbe/Df* late telophase spermatocytes, randomly selected from images taken in five experiments. Scale Bars, 10μm.
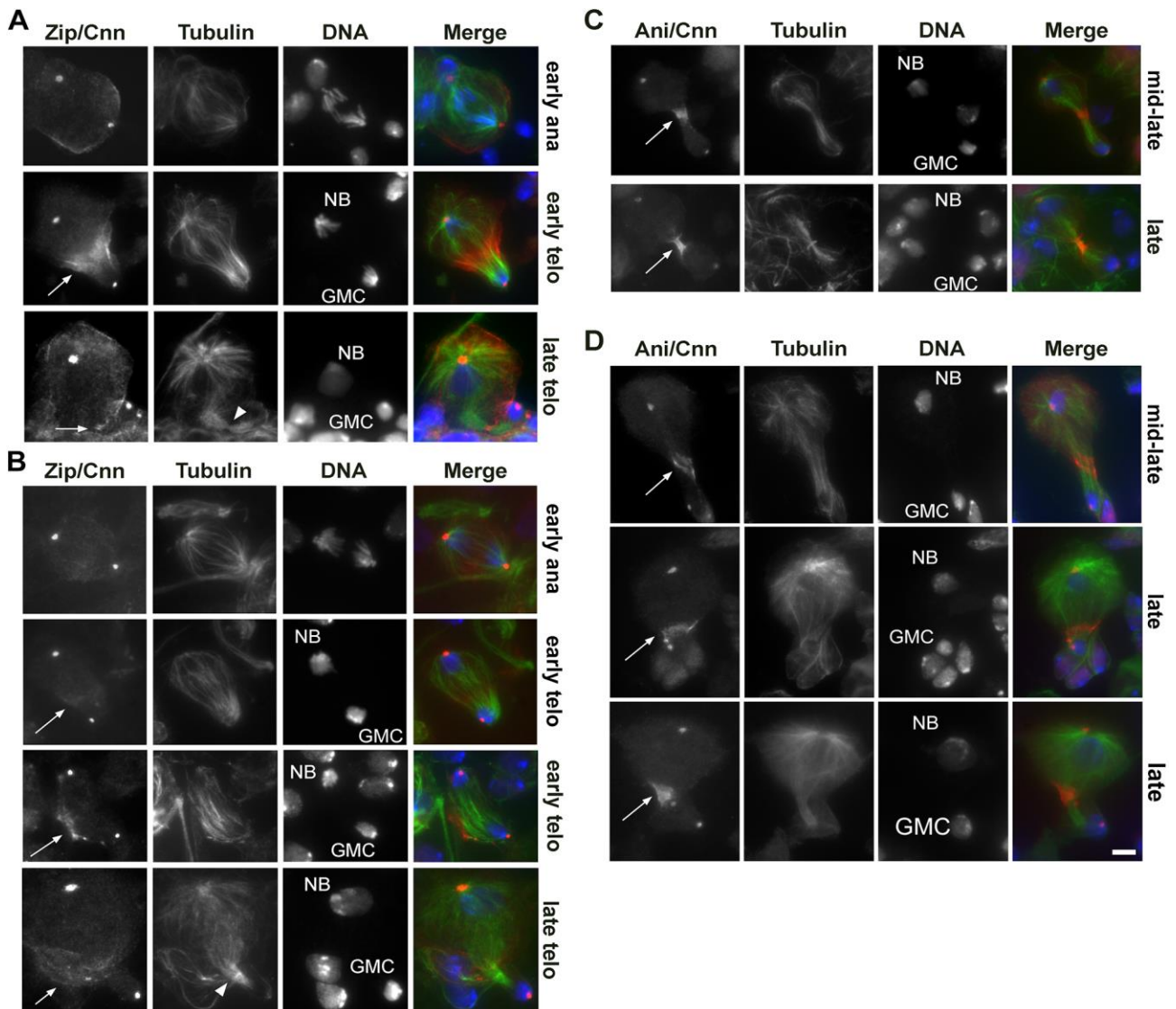
Fig. 3 Dividing neuroblasts from *cbe* mutants display defective contractile rings. (A,B) Wild-type (A) and *cbe^{z2097}/Df(2R)BSC608 (cbe/Df)* (B) mutant neuroblasts during early anaphase, early telophase and late telophase, stained for tubulin (green), DNA (blue) and Zip (red); N= 25 wild-type and *cbe/Df* early anaphase neuroblasts; N=30 wild-type and *cbe/Df* early telophase neuroblasts, N= 50 wild-type and *cbe^{z2097}/Df* late telophase neuroblasts; randomly selected from images taken in five experiments. Arrows point to Zip accumulation, arrowhead points to the central spindle midzone. Note that the spindle midzone is pinched in the middle in wild-type but not in *cbe/Df* late telophase (C,D) Wild-type (C) and *cbe^{z2097}/Df(2R)BSC608 (cbe/Df)* mutant neuroblasts (D) during telophase, stained for tubulin (green), DNA(blue) and Anillin (red); N= 50 wild-type and *cbe/Df* mid-late telophase neuroblasts; N= 40 wild-type and *cbe/Df* late telophase neuroblasts; randomly selected from images taken in seven experiments. Arrows point to Anillin in constricted (wild type) and unconstricted (*cbe/Df*) rings. NB, Neuroblast nucleus; GMC, Ganglion mother cell nucleus. Scale Bar, 5μm.
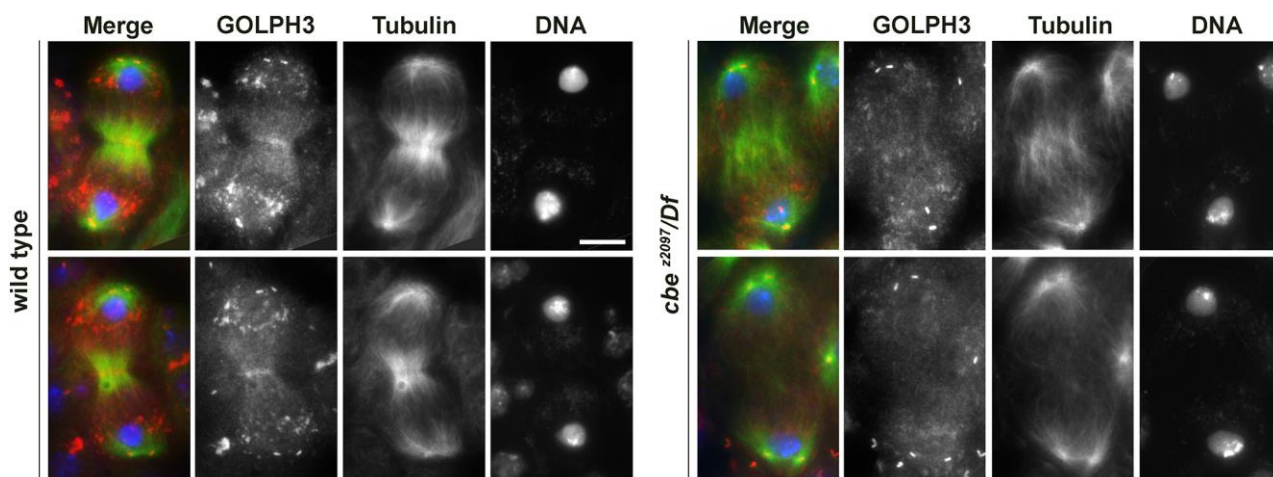
Fig. 4 The *cbe* mutation impairs GOLPH3 accumulation in the cleavage furrow of dividing spermatocytes. Wild-type and *cbe^{z2097}/Df(2R)BSC608 (cbe^{z2097}/Df)* mutant spermatocytes during early- and mid-late telophase, stained for tubulin (green), DNA (blue) and GOLPH3 (red); N=20 wild-type and *cbe^{z2097}/Df* early telophases; N= 30 wild-type and *cbe^{z2097}/Df* mid-late telophases randomly selected from images taken in five experiments. Scale Bar, 10µm.
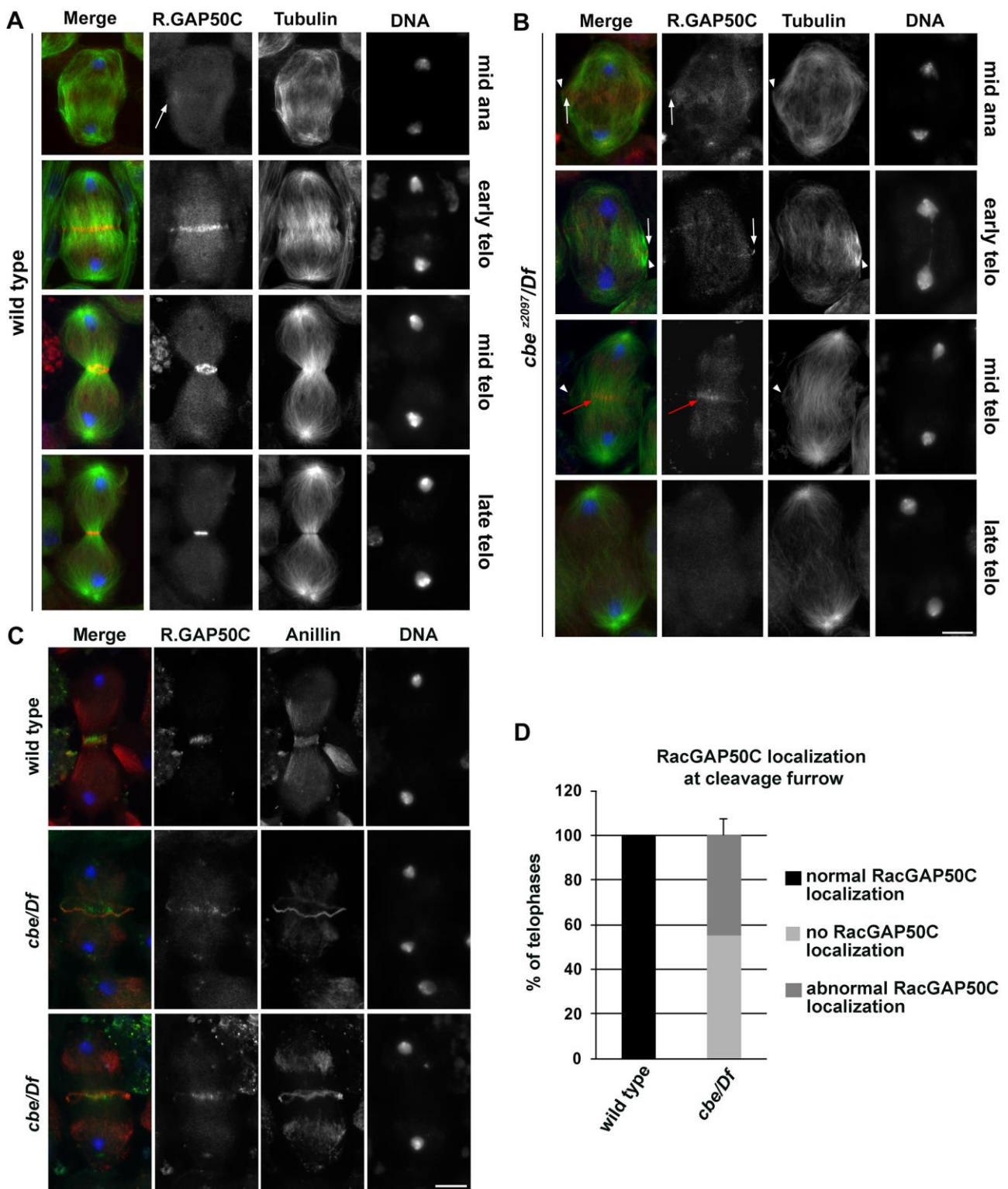
**Fig. 5 Localization of RacGAP50C is disrupted in telophase spermatocytes from *cbe^z2097*
mutant males.** (A,B) Wild-type (A) and *cbe^z2097*/*Df(2R)BSC608 (cbe^z2097*/*Df)* mutant spermatocytes
(B) stained for tubulin (green), DNA (blue) and RacGAP50C (red). N= 18 wild-type and *cbe*/*Df*
mid-anaphases; N=34 wild-type and *cbe*/*Df* early telophases; N= 50 wild-type and *cbe^z2097*/*Df* late
telophases. Note that in late stages of cytokinesis from *cbe^z2097*/*Df*, RacGAP50C either fails to

localize or localizes to interior microtubule bundles of the cell. White arrows point to RacGAP50C accumulation at the peripheral microtubules, arrowhead points to the peripheral microtubules, red arrow points to RacGAP50C at the interior microtubule bundles (C) Wild-type and cbe^{z2097}/Df *(cbe/Df)* mutant spermatocytes stained for RacGAP50C (green), DNA (blue) and Anillin (red). (D) Quantification of defective localization of RacGAP50C in dividing telophase spermatocytes. N=49 wild-type and cbe^{z2097}/Df telophases, randomly selected from images taken in five experiments. Graph shows percentage ±s.d. Scale Bar, 10µm.
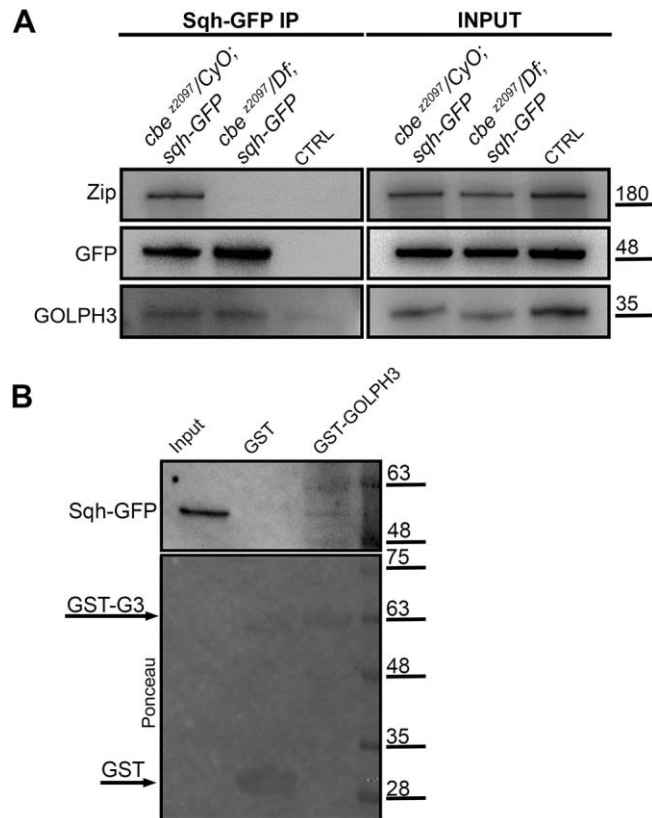
Fig. 6 Co-IP and GST pull-down reveal the interaction of Sqh with Zip and GOLPH3. (A) Protein extracts from testes expressing Sqh-GFP of the indicated genotypes were immunoprecipitated for GFP or control binding beads (CTRL) and blotted for GFP, Zip and GOLPH3. Testis extracts from Sqh-GFP males were used in control experiments (CTRL). 2% of the total lysate (Input) and one third of the immunoprecipitates were loaded and probed with the indicated antibodies. Molecular masses are in kilodaltons. The Co-IP was performed three times with identical results. ((B) GST-GOLPH3 but not GST precipitated Sqh-GFP from testis extracts. Ponceau staining is shown as a loading control. 2% of the input and 25% of the pull-down were loaded and probed with the indicated antibodies. Molecular masses are given in kilodaltons.
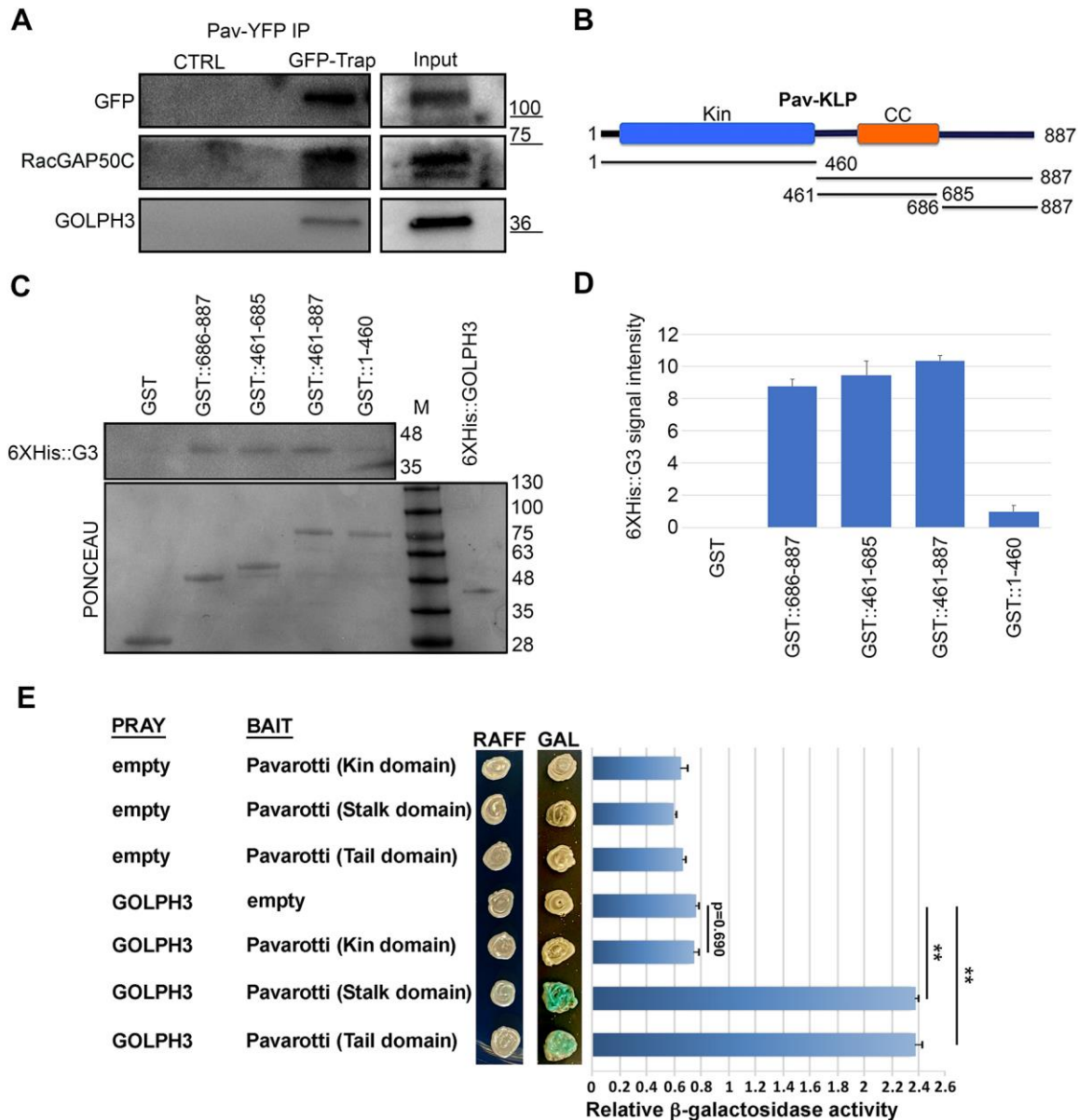
Fig. 7. GOLPH3 binds to Pav protein. (A) RacGAP50C and GOLPH3 coprecipitate with Pav-YFP. Protein extract from testes expressing Pav-YFP was split in half and immunoprecipitated with either GFP trap or control beads (CTRL) and blotted for YFP, RacGAP50C and GOLPH3. 2% of the total lysate (Input) and one third of the immunoprecipitates were loaded and probed with the indicated antibodies. Molecular masses are in kilodaltons. The Co-IP was performed three times with identical results. (B) Schematic of Pav domains. aa 1-460: motor domain (Kin); aa 461-685: coiled-coil domain (Stalk); aa 686-887: C-terminal domain (Tail). (C) The three domains of Pav, plus the combination Stalk+Tail (aa 461-887) were expressed as GST tagged proteins and tested for binding to 6XHis::GOLPH3 (6XHis::G3) Recombinant GST-Pav proteins, immobilized on glutathione beads were incubated with recombinant 6XHis-tagged GOLPH3. The amount of 6XHis-tagged GOLPH3 that directly bound to each GST-Pav protein or to GST was detected with anti-6XHis antibodies..

Ponceau staining is shown as a loading control. 0.1% of the input and 25% of the pull-down were loaded and probed with anti-6XHis antibodies. Molecular masses are in kilodaltons (D) Graph represents quantification of 6XHis-tagged GOLPH3 bound to each form of Pav by western blot. Protein band intensities were obtained from three independent experiments. Data are means ±s.d. (E) Y2H assay to test GOLPH3 interaction with Pav domains. Only the Stalk and Tail domains induce LacZ expression (blue colour indicates positive interaction). Quantification of LacZ reporter expression (graph) with different combinations of bait and prey plasmids is shown. See materials and methods for further details. Error bars, s.e.m. Statistically significant difference is **p <0.01 (Mann–Whitney U test). RAFF, raffinose; GAL, galactose.
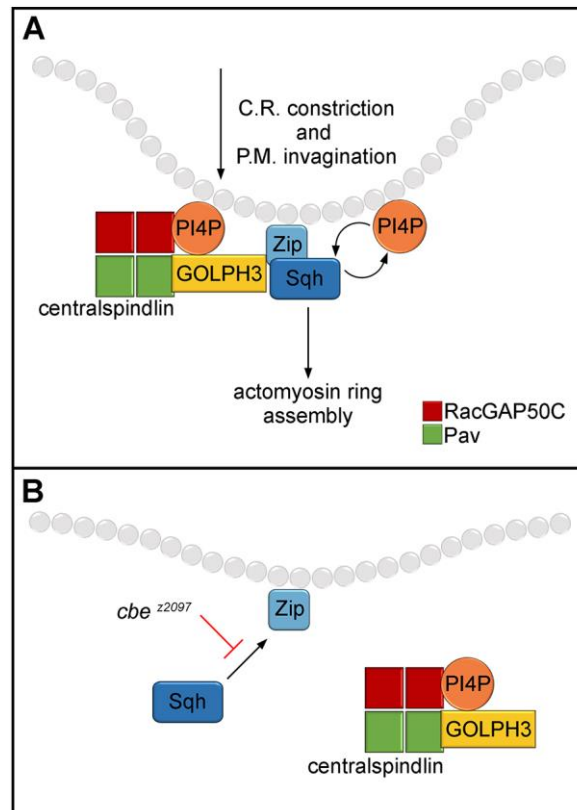
Fig. 8 Diagram depicting the reciprocal dependence of Myosin and PI(4)P-GOLPH3 during early stages of cytokinesis. (A) In dividing wild-type cells, binding of Zip protein to Sqh is required for robust actomyosin ring assembly at the cleavage site. The Zip/Sqh complex interacts with GOLPH3 protein and enables localization of GOLPH3 and presumably of PI(4)P at the cleavage site. In turn, GOLPH3 controls centralspindlin maintenance at the invaginating plasma membrane by binding to C-terminal domains of the Pav subunit. Centralspindlin localization at furrow plasma membrane is also stabilized by the interaction of RacGAP50C with polyanionic phosphoinositide lipids, including PI(4)P. (B) in *cbe* mutants Zip is unable to bind Sqh protein. As a consequence, GOLPH3 fails to accumulate at the cleavage site resulting in failure to maintain centralspindlin at the invaginating plasma membrane and to undergo cleavage furrow ingression.

Supplementary Information

Figure S1

Figure S1. Western blot analysis from *cbe^{z2097}/Df(2R)BSC608* mutants. Western blot from adult testis (testes) or larval brain extracts (brains). Polyclonal antibodies against Zip protein recognized a band of 200kDa that is reduced in extracts from *cbe^{z2097}/Df(2R)BSC608 (cbe)* mutants compared with *Df(2R)BSC608/+* control siblings (CTRL). α-tubulin (Tubulin) was used as a loading control. Molecular masses are given in kilodaltons. (B) Quantification of the expression level of Zip protein in western blots from adult testis (testes) and larval brain (brains) extracts using Image J software; N=3 independent experiments. The intensity of each band relative to the intensity of the loading control (α-tubulin) was normalized to the CTRL (*Df(2R)BSC608/+*). Data are means ±s.d. Statistically significant differences, **p<0.01; ***p<0.0001 (unpaired Student's *t*-test).

Figure S2

Figure S2. Formation of F-actin rings fails in spermatocytes from *cbe/Df* males. Wild type and *cbe*^{z2097}/Df spermatocytes during mid- (M) and late telophase (L) were stained to visualize tubulin (green), F-actin (red) and DNA (blue). N=28 wild-type and *cbe/Df* mid telophases; N= 40 wild-type and *cbe/Df* late telophases, randomly selected from images taken in five experiments. Scale Bar, 10μm.
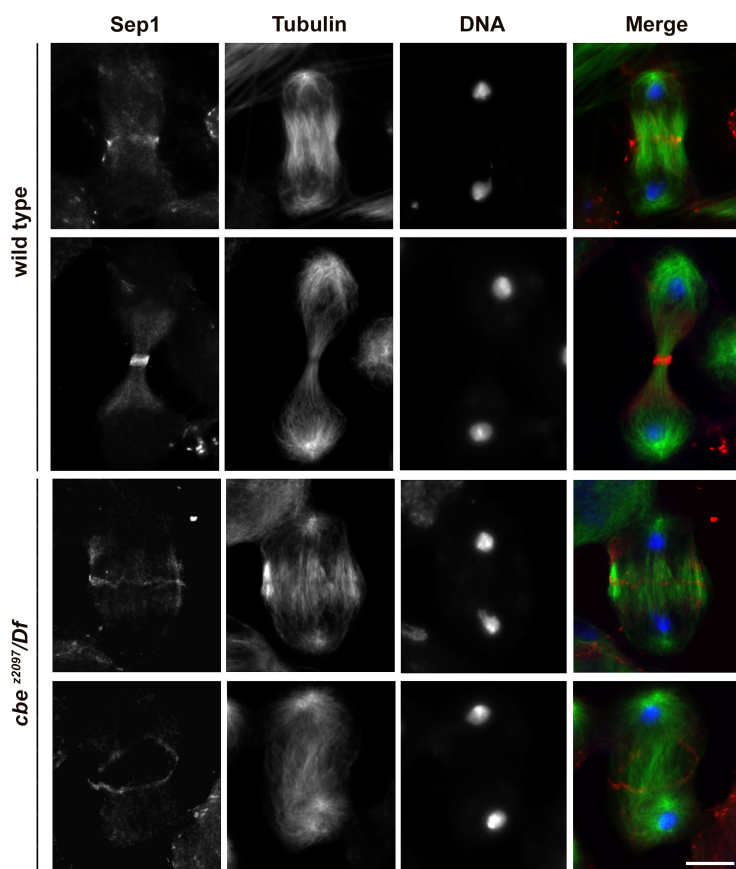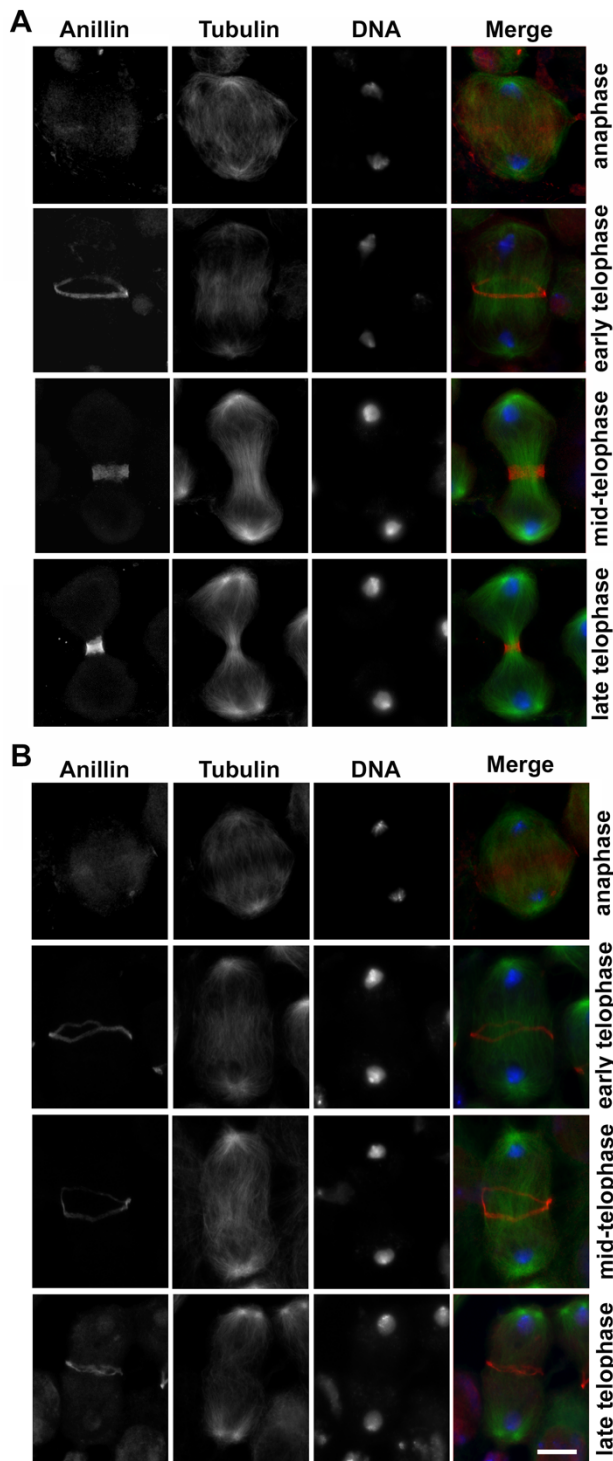
Figure S3

	Sep1	Tubulin	DNA	Merge

(rows labeled: wild type, wild type, *cbe*^{z2097}/*Df*, *cbe*^{z2097}/*Df*)

Figure S3. Zip is required for stabilizing Septin rings at the equatorial cortex of dividing spermatocytes. Wild-type and *cbe*^{z2097}/*Df(2R)BSC608* (*cbe*^{z2097}/*Df*) mutant spermatocytes during early telophase and late telophase, stained for tubulin (green), DNA (blue) and Sep1 (red). N=25 wild-type and *cbe*^{z2097}/*Df* early telophase spermatocytes; N=38 wild-type and *cbe*^{z2097}/*Df* late telophase spermatocytes; randomly selected from images taken in five experiments. Scale Bar, 10μm.
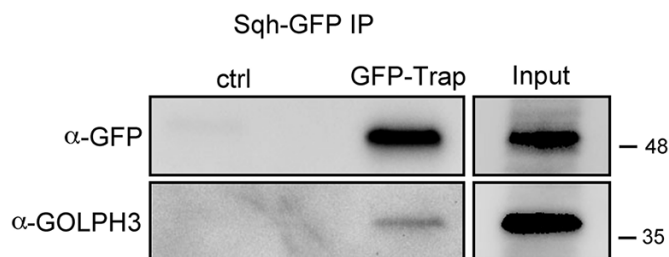
Figure S4

Figure S4. Constriction of Anillin rings fails in spermatocytes from *cbe/Df* males. (A) Wild-type and (B) *cbe^{z2097}/Df(2R)BSC608* (*cbe^{z2097}/Df*) mutant spermatocytes during anaphase and telophase, were stained for tubulin (green), DNA (blue) and Anillin (red). N=22 wild-type and *cbe^{z2097}/Df* early anaphase spermatocytes; N=25 wild-type and *cbe^{z2097}/Df* early telophase spermatocytes; N=32 wild-type and *cbe^{z2097}/Df* mid-telophase spermatocytes; N=36 wild-type and *cbe^{z2097}/Df* late telophase spermatocytes; randomly selected from images taken in six experiments. Scale Bar, 10μm.

Figure S5

Figure S5. GOLPH3 co-precipitates with Sqh in testes. Protein extract from testes expressing Sqh-GFP was split in half and immunoprecipitated with either GFP-trap or control binding beads (ctrl) and blotted for GFP and GOLPH3. 2% of the total lysate (Input) and one third of the immunoprecipitates were loaded and probed with the indicated antibodies. Molecular masses are in kilodaltons. The Co-IP was performed three times with identical results.
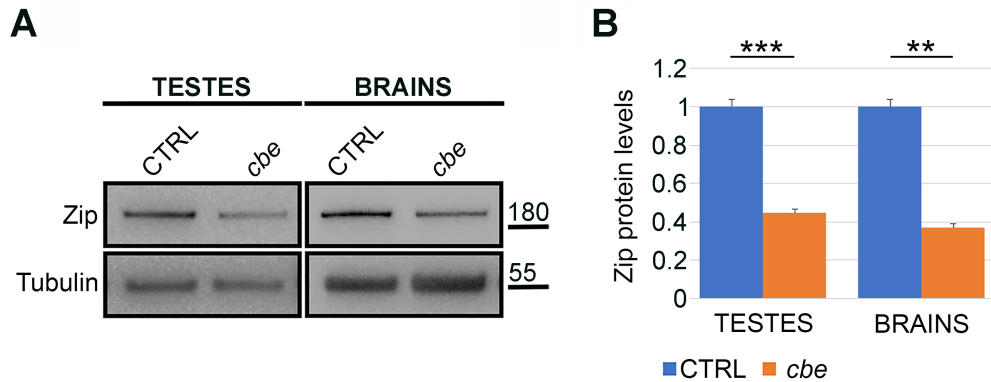
Supplementary Information

Figure S1

Figure S1. Western blot analysis from *cbe^{z2097}/Df(2R)BSC608* mutants. Western blot from adult testis (testes) or larval brain extracts (brains). Polyclonal antibodies against Zip protein recognized a band of 200kDa that is reduced in extracts from *cbe^{z2097}/Df(2R)BSC608 (cbe)* mutants compared with *Df(2R)BSC608/+* control siblings (CTRL). α-tubulin (Tubulin) was used as a loading control. Molecular masses are given in kilodaltons. (B) Quantification of the expression level of Zip protein in western blots from adult testis (testes) and larval brain (brains) extracts using Image J software; N=3 independent experiments. The intensity of each band relative to the intensity of the loading control (α-tubulin) was normalized to the CTRL (*Df(2R)BSC608/+*). Data are means ±s.d. Statistically significant differences, **p<0.01; ***p<0.0001 (unpaired Student's *t*-test).

Figure S2

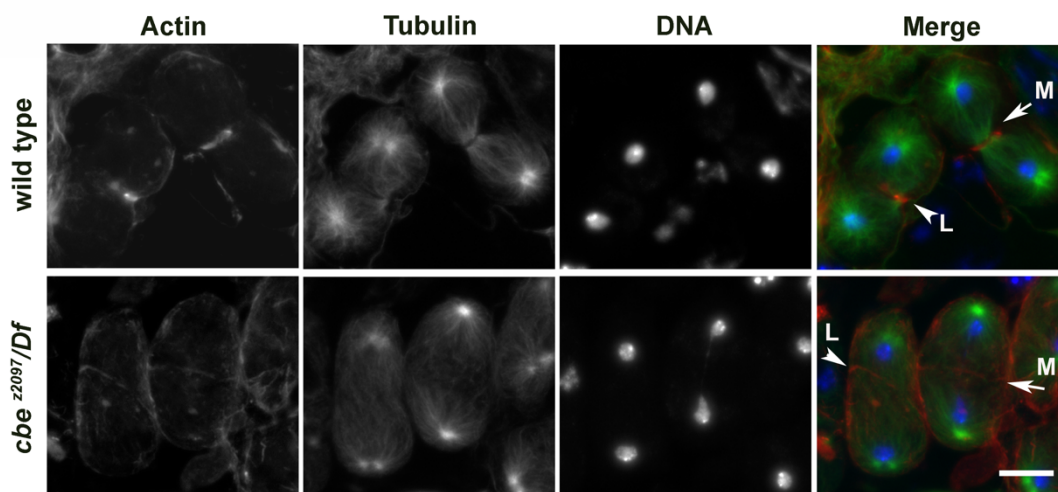**Figure S2. Formation of F-actin rings fails in spermatocytes from *cbe/Df* males.** Wild type and *cbe^{z2097}*/Df spermatocytes during mid- (M) and late telophase (L) were stained to visualize tubulin (green), F-actin (red) and DNA (blue). N=28 wild-type and *cbe/Df* mid telophases; N= 40 wild-type and *cbe/Df* late telophases, randomly selected from images taken in five experiments. Scale Bar, 10µm.
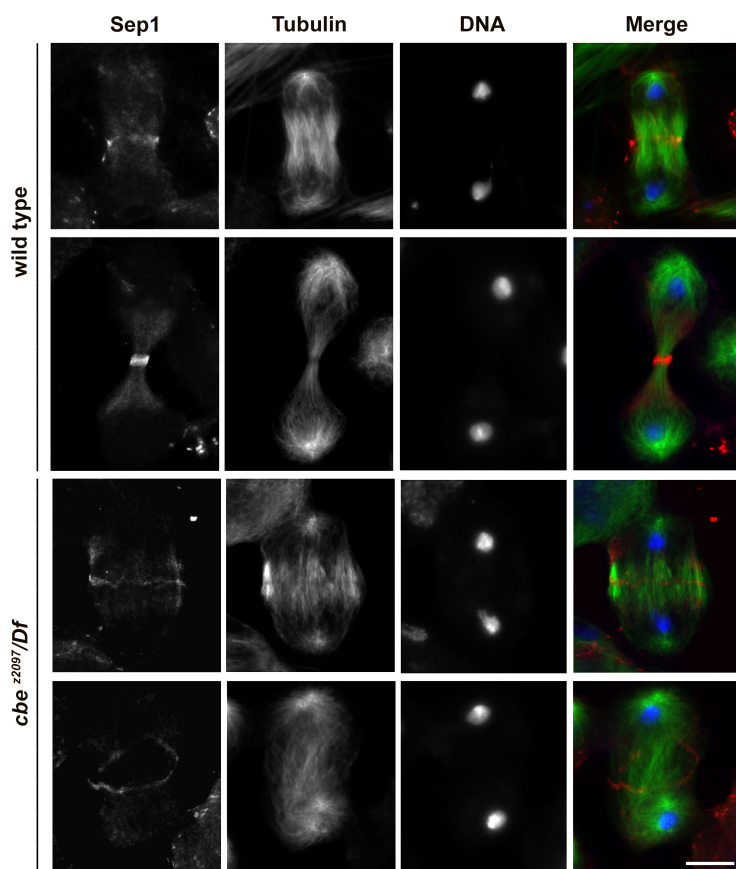
Figure S3

Figure S3. Zip is required for stabilizing Septin rings at the equatorial cortex of dividing spermatocytes. Wild-type and $cbe^{z2097}/Df(2R)BSC608$ (cbe^{z2097}/Df) mutant spermatocytes during early telophase and late telophase, stained for tubulin (green), DNA (blue) and Sep1 (red). N=25 wild-type and cbe^{z2097}/Df early telophase spermatocytes; N=38 wild-type and cbe^{z2097}/Df late telophase spermatocytes; randomly selected from images taken in five experiments. Scale Bar, 10μm.
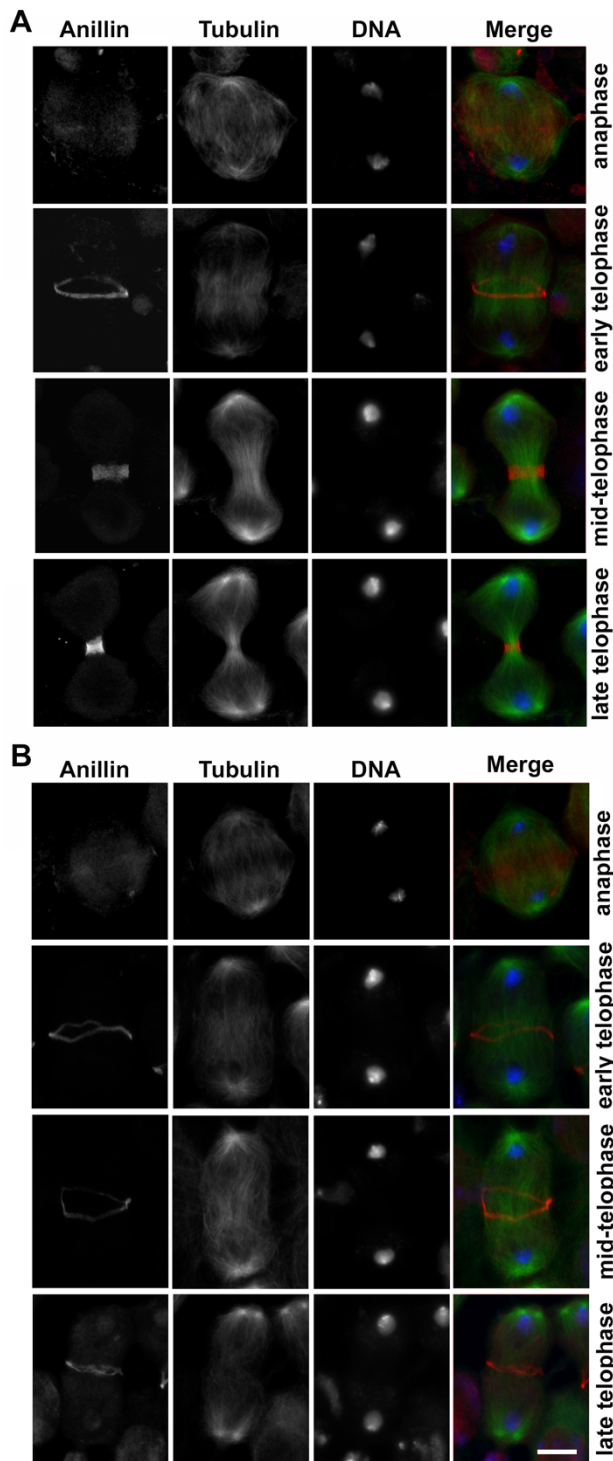
Figure S4

Figure S4. Constriction of Anillin rings fails in spermatocytes from *cbe/Df* males. (A) Wild-type and (B) *cbe^z2097^/Df(2R)BSC608* (*cbe^z2097^/Df*) mutant spermatocytes during anaphase and telophase, were stained for tubulin (green), DNA (blue) and Anillin (red). N=22 wild-type and *cbe^z2097^/Df* early anaphase spermatocytes; N=25 wild-type and *cbe^z2097^/Df* early telophase spermatocytes; N=32 wild-type and *cbe^z2097^/Df* mid-telophase spermatocytes; N=36 wild-type and *cbe^z2097^/Df* late telophase spermatocytes; randomly selected from images taken in six experiments. Scale Bar, 10μm.
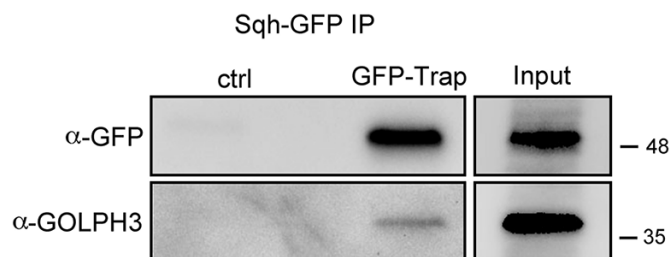
Figure S5

Figure S5. GOLPH3 co-precipitates with Sqh in testes. Protein extract from testes expressing Sqh-GFP was split in half and immunoprecipitated with either GFP-trap or control binding beads (ctrl) and blotted for GFP and GOLPH3. 2% of the total lysate (Input) and one third of the immunoprecipitates were loaded and probed with the indicated antibodies. Molecular masses are in kilodaltons. The Co-IP was performed three times with identical results.